

AUS Repository

Design and Implementation of a Cable Robot for Rehabilitation

Item Type	Thesis
Authors	Latifi, Mohammad
Download date	2026-03-16 05:20:30
Link to Item	http://hdl.handle.net/11073/25161

DESIGN AND IMPLEMENTATION OF A CABLE ROBOT FOR
REHABILITATION

by
Mohammad Latifi

A Thesis presented to the Faculty of the
American University of Sharjah
College of Engineering
In Partial Fulfilment
of the Requirements
for the Degree of

Master of Science in
Mechatronics Engineering

Sharjah, United Arab Emirates

December 2022

Declaration of Authorship

I declare that this thesis is my own work and, to the best of my knowledge and belief, it does not contain material published or written by a third party, except where permission has been obtained and/or appropriately cited through full and accurate referencing.

Signed.....Mohammad Latifi.....

Date.....10/12/2022.....

The Author controls copyright for this report.

Material should not be reused without the consent of the author. Due acknowledgement should be made where appropriate.

© Year 2022

Mohammad Latifi

ALL RIGHTS RESERVED

Approval Signatures

We, the undersigned, approve the Master's Thesis of Mohammad Latifi

Thesis Title: Design and Implementation of a Cable Robot for Rehabilitation

Date of Defence: 19th December 2022

Name, Title and Affiliation

Signature

Dr. Lotfi Romdhane

Professor, Department of Mechanical Engineering

Thesis Advisor

Dr. Mohammad Jaradat

Professor, Department of Mechanical Engineering

Thesis Co-Advisor

Dr Mehdi Ghommem

Associate Professor, Department of Mechanical Engineering

Thesis Committee Member

Dr. Shayok Mukhopadhyay

Associate Professor, Department of Electrical Engineering

Thesis Committee Member

Dr. Mamoun AbdelHafez

Program Coordinator

Mechatronics Engineering Program

Dr. Lotfi Romdhane

Associate Dean for Graduate Affairs and Research

College of Engineering

Dr. Fadi Aloul

Dean

College of Engineering

Dr. Mohamed El-Tarhuni

Vice Provost for Research and Graduate Studies

Office of Research and Graduate Studies

Acknowledgements

I would like to thank my advisors Dr. Lotfi Romdhane and Dr. Mohammad Jaradat for providing knowledge, guidance, support, and motivation throughout my research stages. I'm deeply beholden for their great assistance, worthy discussion, and suggestions.

I am also grateful and honour that I have been awarded assistantship to work as a graduate teaching assistant form American University of Sharjah while pursing my studies in mechatronic engineering master program.

Dedication

To all who are humbled in way of aiding others.

Abstract

Due to the precision and repeatability that current robotic system offer; many researchers and innovators have proposed solution for biomedical needs and applications. Classical robots can offer great precision and offer a high payload-to-weight mechanism to handle different biomedical tasks. Nonetheless, the classical robots might act poorly where the adaptability and flexibility of the system is challenged. One way of tackling these issues is to use Cable-Driven Parallel Robot (CDPR) to address all the issues raised by the performance measures mentioned earlier. Due to the flexible links used in CDPR, the control of the system becomes a challenging problem and many researchers have developed different solutions to overcome many modeling problems, including unilateral condition, where links of the robot will be actuated only upon pulling an object. Under the studies that have been done for this thesis work, a CDPR robot has been prototyped with a control joint scheme, where the motion of the robot has been set through Geometric Inverse Kinematic (GIK), and the motors are controlled through PID control that receives feedback from each motor encoder. Later in this study, the performance of the system has been studied under 11 different cases under different trajectory conditions. It has been shown that the best steady state is achieved when the robot has the smallest acceleration or deceleration among the via points, which gives the Integral Square Error (ISE) value of 25.3. The transient response, however, has the best performance when a lower number of via points has been selected for a given path, which gives the Integrated Time Absolute Error (ITAE) of 706.2. The system performs the trajectory planning in absence of high-level control or encountering errors introduced by model measurement inaccuracies

Keywords: Parallel Cable Robot, Rehabilitation, Geometric Inverse Kinematic, Parallel Robot, Cable Robot

Contents

Abstract	6
List of Figures	8
List of Tables	10
Chapter 1. Introduction.....	11
1.1. Overview.....	11
1.2. Research Contribution.....	13
1.3. Thesis Organization	13
Chapter 2. Literature Review.....	14
2.1. Head-Neck Rehabilitation.....	14
2.2. Suspended Parallel Cable Robot in Rehabilitation	17
2.3. Cable Driven Parallel Manipulators.....	18
Chapter 3. Design and Modelling.....	20
3.1. Design of Cable Robot Biomedical.....	20
3.2. Cable Mechanism.....	22
3.3. Inverse Kinematic Model.....	25
3.4. Rotation to Planar Movement Mapping	27
Chapter 4. Experiment Methodology	28
4.1. Experimental Setup.....	28
4.2. Model Validation and Error Analysis	34
4.2.1. Case 1.....	34
4.2.2. Case 2.....	38
4.2.3. Case 3.....	39
4.2.4. Case 4.....	40
4.2.5. Case 5.....	41
4.2.6. Case 6.....	42
4.2.7. Case 7.....	43
4.2.8. Case 8.....	44
4.2.9. Case 9.....	45
4.2.10. Case 10.....	49
4.2.11. Case 11.....	50
4.2.12. Discussion	54
Chapter 5. Conclusion	57
Vita	63

List of Figures

Figure 1: Robots kinematic chains: (a) Parallel manipulator, (b) Serial manipulator [1]	11
Figure 2: CDRMs examples: (a) tendon based robot, (b) suspended cable robot [2]	12
Figure 3: Division of human based on musculoskeletal system [4]	13
Figure 4: Human body planes [5]	13
Figure 5: 3-RRS active brace [10]	14
Figure 6: Carneck rehabilitation robot [11].....	15
Figure 7: Lingampally and Selvakumar 3-RPS rehabilitation robot [12].....	15
Figure 8: 3-RPS Robot design [13].....	15
Figure 9: RXS robot for human head-neck rehabilitation [16]	16
Figure 10: 6 revolute axis serial robot rehabilitation robot [15]	16
Figure 11: Cable driven rehabilitation robot forlegs [20]	17
Figure 12: Cable-driven rehabilitation robot for arm [21].....	17
Figure 13: A reconfigurable cable driven robot [22]	17
Figure 14: Types of CDPR based on degrees of freedom [23]	18
Figure 15: Steward parallel robot [23]	18
Figure 16: Type of human movement[35]	21
Figure 17: Neck flexion [36].....	22
Figure 18: Neck extension [36].....	22
Figure 19: Outlets: (a) eyelet, (b) single-pulley, (c) double-pulley, (d) multi-pulley [37].	22
Figure 20: Cable robot rehabilitation	23
Figure 21: 1R2T cable robot without intermediate stage.....	24
Figure 22: Motor pulley end effector	25
Figure 23: Vector Representation of the system	26
Figure 24: Conical section corresponding for certain angle movement.....	27
Figure 25: Performance chart of MX64-at graph [39]	29
Figure 26: Robot structure	30
Figure 27: Motor model with pulley	30
Figure 28: Motor pulley and idler pulley	30
Figure 29: Parallel cable robot: (a) Top view, (b) side view.....	30
Figure 30: Motor communication network with PC	31
Figure 31: Platform dimensions	31
Figure 32: Opti track configuration	32
Figure 33: Opti-Track calibration results.....	33
Figure 34: Dynamixel PID controller [39].....	34
Figure 35: Infinity along y trial planar movement case 1	35

Figure 36: Motor angular position trajectory case 1	35
Figure 37: Rotary speed vs time for case 1	36
Figure 38: Motor current measurements for the case 1.....	36
Figure 39: Error measurements of case 1.....	37
Figure 40: ITAE errors generated in case 1	37
Figure 41: IAE error generated in case 1	37
Figure 42: ISE error analysis in case 1.....	38
Figure 43: Infinity along x trial planar movement case 2	39
Figure 44: Infinity along x trial planar movement case 3	40
Figure 45: Infinity along x trial planar movement case 4	41
Figure 46: Infinity along x trial planar movement case 5	42
Figure 47: Path generated in case 6	43
Figure 48: Path generated in case 7	44
Figure 49: Robot path for the case 8.....	45
Figure 50: Case 9: study of two circles.....	45
Figure 51: Experiment 1 motor positioning case 9.....	46
Figure 52: Experiment 2 motor positioning case 9.....	46
Figure 53: Rotary speed of experiment 1 & 2 case 9.....	47
Figure 54: Current profiles of case 9	47
Figure 55: Error signal of case 9.....	48
Figure 56: ITAE analysis for case 9.....	48
Figure 57: IAE analysis for case 9.....	48
Figure 58: ISE analysis for case 9.....	49
Figure 59: Path generated in case 10	50
Figure 60: Rectangular Path case 11.....	50
Figure 61: Experiment 1 case 11.....	51
Figure 62: Experiment 2 case 11.....	51
Figure 63: Experiment 3 case 11.....	51
Figure 64: Rotary speed of motor case 11	52
Figure 65: Current profile in case 11	52
Figure 66: Error signal in case 11	53
Figure 67: ITAE analysis for case 11.....	53
Figure 68: IAE analysis for case 11	53
Figure 69: ISE analysis for case 11.....	54

List of Tables

Table 1: Head-neck range of motion [35].....	21
Table 2: Type of cable robots	23
Table 3: MX64-AT motor parameters [39].....	29
Table 4: Planar parameter of the cable robot	31
Table 5: PID gains	33
Table 6: Summary of cases studied.....	34
Table 7: Error performance measures comparison	55
Table 8: Mean square error for the different experiments	55

Chapter 1. Introduction

In this Chapter, the fundamental concepts needed for understanding rehabilitation, musculoskeletal system, and cable-driven robot will be introduced. Furthermore, the contribution and the objective of the study will also be introduced. The end of this chapter will discuss the organization of this document and the objectives of each chapter.

1.1. Overview

Robots have assisted humans to perform certain tasks under better control and with enhanced capability that cannot be attained by humans or by simple mechanisms. With this consideration, robots often face different limitations and challenges due to their characteristics or the environment, in which the robot should operate. Earlier version of the robots is known to have a rigid body structure, which is beneficial in terms of robot modeling and mechanical rigidity. There are different classifications of classical robots, based on their kinematic chains. Classical robots' manipulators are divided into serial manipulator (Figure 1), which has open-loop kinematic chain, and parallel manipulators, which have closed loop kinematic chain. Serial manipulators known to have a larger workspace compared to parallel manipulators and in terms of mathematical modeling are easier compared to parallel robots; however serial manipulators suffer from positioning error near workspace extreme points [1]. Parallel robots, on the other hand offer a better accuracy of desired way paths and offer higher payload-to-weight parameters, which will reduce energy consumption of the system [1].

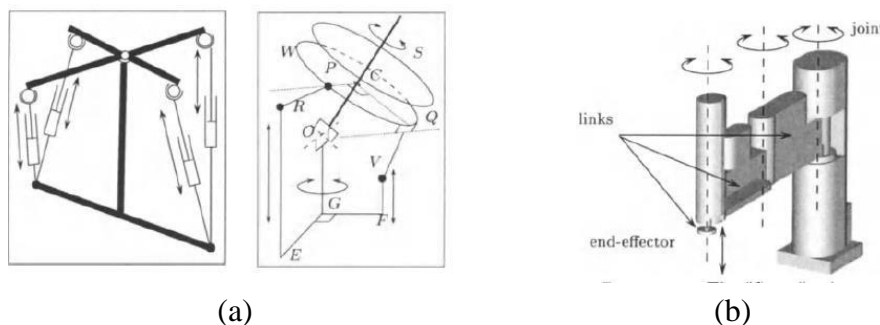


Figure 1: Robots kinematic chains: (a) Parallel manipulator, (b) Serial manipulator [1]

One class of solution to the existed problems in the classical rigid bodies are Cable-Driven Robotic Manipulators (CDRM). CDRMs are generally classified into tendon-driven robots and suspended cable-driven robots. Tendon robots are a class of CDRMs,

where a rigid link movement is dependent on the length of some cables attached to it [2]. Interaction of the tendons with rigid bodies are usually through pulleys which are mounted at the base of the robot. Suspended cables robots are a class of CDRM, which use the gravity to ensure the equilibrium of the end effector. [2]. Examples of tendon based robots and suspended cable robot are in Figure 2.

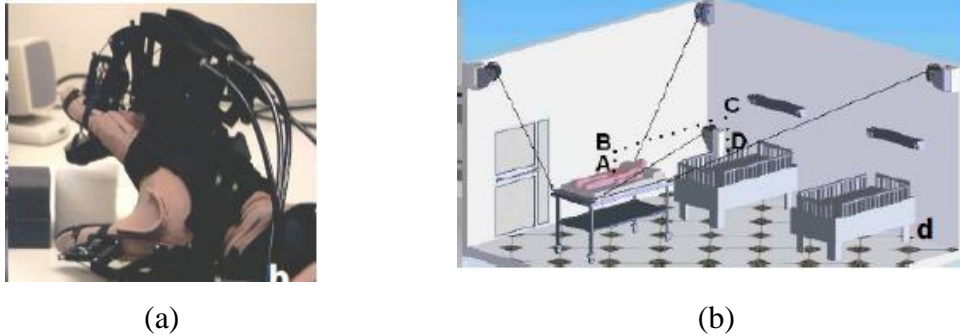


Figure 2: CDRMs examples: (a) tendon based robot, (b) suspended cable robot [2]

One of the most used applications of the CDRM is in the rehabilitation of human body due to better cost reduction, time-effectiveness, and better repeatability compared to manual rehabilitation training [2], [3]. The rehabilitation process between CDRM is in two levels: physical human-robot interaction (pHRI), and cognitive human-robot interaction (cHRI) [3].

Rehabilitation of the musculoskeletal system is divided into two major parts: the axial body, and the appendicular body [4] as it has been shown in Figure 3. The axial body covers muscles and skeletal parts of the head, neck, and trunk of the human body. The appendicular body covers the upper extremity and lower extremity of the human body. The upper extremity covers parts such as the shoulder girdle, arm, forearm, and hand. The lower extremity covers the pelvis, thigh, leg, and foot. The movements of the human body are described in three different and perpendicular planes, which all pass through the human center of gravity, that is, the sagittal plane, transverse plane, and frontal plane [5] in Figure 4. The sagittal plane is the one where human part are divided into left and right, and movement in this plane are termed flexion and extension. The transverse plane divide's human part into top and bottom part, and movement in this plane is referred as rotation. Frontal plane divide's human part into front and back parts, and movement along this plane referred as abduction and adduction.

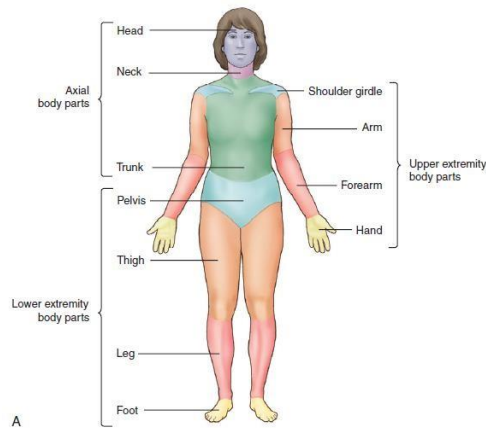


Figure 3: Division of human based on musculoskeletal system [4]

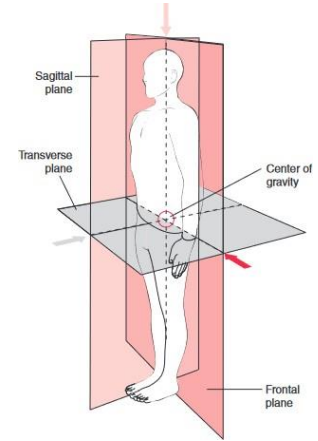


Figure 4: Human body planes [5]

Through the literature survey, it has been although extensive research and development are available in Cable-Driven Robotic Manipulators (CDRM) for upper extremity and lower extremity, there has been a modest development in rehabilitation of axial body parts, particularly head-neck musculoskeletal system. With the aim of improvement in rehabilitation process through application of robotics, a new parallel end-effector based CDRM is proposed and aim of this research is to develop mathematical modeling and control scheme of the CDRM as well as design and develop the physical apparatus on clinical level to measure the performance of the system.

1.2. Research Contribution

Objective of this research is to develop a CDRM, such that it can mimic the human head-neck motion. The objectives of this thesis can be summarized as follows:

- Design a CDRM, which can help in the rehabilitation of the head-neck joint
- Develop a mathematical model of CDRM, to simulate the different tasks
- Build a prototype and test different control strategies experimentally.

1.3. Thesis Organization

This document shall first discuss about available head-neck rehabilitation robotics in literature and later discusses about available parallel cable robot and significant works that has been done in modelling and control of the system. In next section necessary mathematics of the cable driven robots has been introduced and a preliminary design has been illustrated, which will be experimentally deployed in later stage of the research. In last section a conclusion statement followed by future has been discussed.

Chapter 2. Literature Review

The previous studies in literature have shown the prominent effect of precision and repeatability of the robot in biomedical applications, particularly regarding rehabilitation process. The novel technology in robotics have introduced more flexibility to the system and particularly, the parameters of the system can be adjusted. This chapter will review previous works that has been done in the field of head-neck rehabilitation, and the robotics used for this purpose.

2.1. Head-Neck Rehabilitation

Studies has proven that activity-based rehabilitation is one principal strategy to promote functional recovery after a neurological injury, such as Spinal Cord Injury (SCI), Head-Neck Cancer (HNC), and stroke [6], [7]. Robotic rehabilitation would assist the therapist in increasing the number of repetitions in physiotherapy sessions, which ultimately leads to better results in achieving rehabilitation objectives [6]. There has been extensive research on application of robotics upper extremity and lower extremity rehabilitation [8], [9]. Several studies have focused on the application of the rehabilitation robotic on head-neck joint. As shown in Figure 5 Zhang *et al.* designed a spring-loaded compliant mechanism with kinematic topology of 3-RRS (Revolute Spherical) to mimic the human head-neck motion for dropped head syndrome (DHS) rehabilitation process [10]. Spring actuators in the previous study are responsible for moving the head-neck position to the desired trajectory, which is a significant advantage not only compared to static braces, but also a characteristic which can be used in rehabilitation.

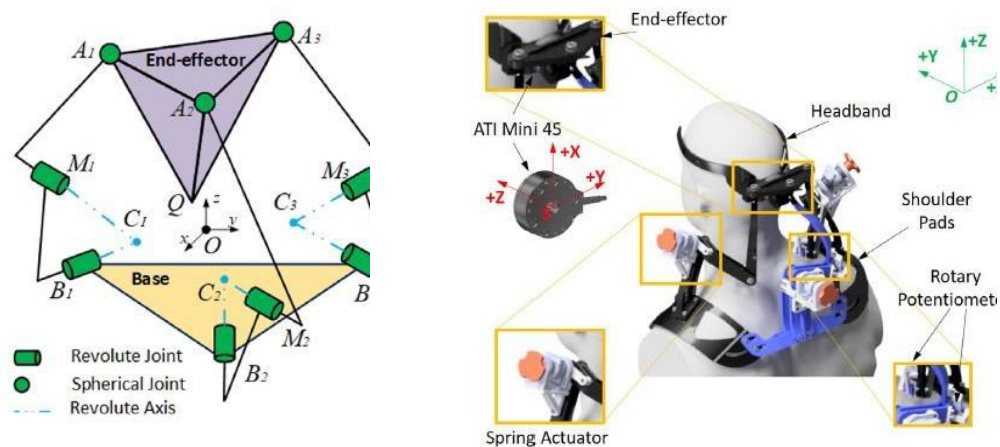


Figure 5: 3-RRS active brace [10]

Shoaib *et al.* has developed a tendon-based cable-driven neck rehabilitation robot (Figure 6), which has two on-link and one hybrid type of antagonistic cable driven joints and offers 3 degrees of freedom [11]. In their study they investigated the wrench closure workspace, but no control scheme has been developed to prevent unwanted behavior.

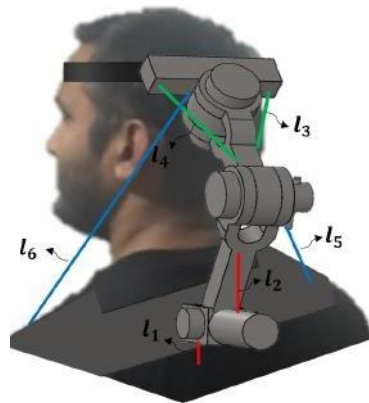


Figure 6: Carneck rehabilitation robot [11]

Lingampally and Selvakumar have developed a parallel 3-RPS (Revolute Prismatic Spherical) robotic manipulator (Figure 7) to perform rehabilitation [12]. Furthermore, through an experiment they have studied the workspace of their robot and verified with their mathematical model. Ibrahim *et al.* also developed a 3-RPS system (Figure 8) which tracks the head neck motion as well as supports the head-neck position for a given pose [13].

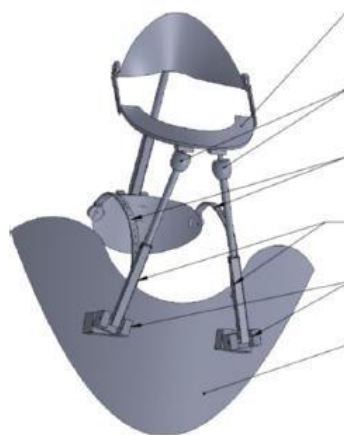


Figure 7: Lingampally and Selvakumar 3-RPS rehabilitation robot [12]

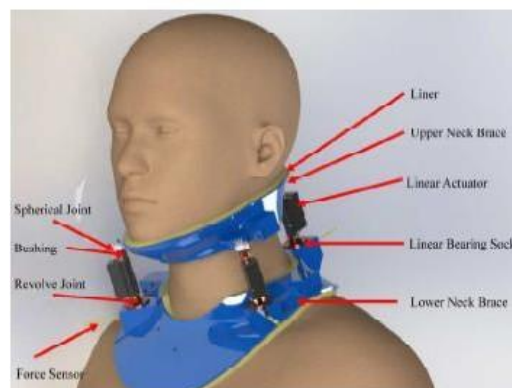


Figure 8: 3-RPS Robot design [13]

Liu *et al.* designed a robot with 3-RXS mechanism (Figure 9) that provides a smoother motion for patient in order to avoid any secondary injuries while rehabilitating the head-neck musculoskeletal system [14]. In their study they have performed finite element analysis over the compliant hinges to make sure that the head-neck desired motion resides within the robot workspace.



FIGURE 17: 3-RXS mechanism prototype.

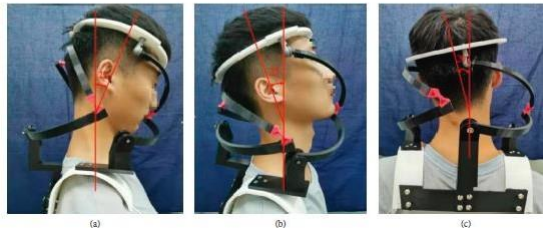


Figure 9: RXS robot for human head-neck rehabilitation [16]

Chang *et al.*, inspired by the first 6 vertebrae of human neck, provided a six revolute joint mechanism robot (Figure 10) that has 6 degrees of freedom [15]. Later in their study they performed a pilot study with EMG to measure muscle activities and evaluates head-neck movement of the patient at the musculoskeletal level.



Figure 10: 6 revolute axis serial robot rehabilitation robot [15]

Using rigid links in the design of rehabilitation robots might result in wrong movements of the head-neck as the robot is not adjustable hence cannot adjust to the differences in dimensions of patients. For this purpose, some researchers proposed new designs based on cable robots. These robots have the advantage of being light and less intrusive, which would increase the acceptability of such devices by the patients. Utilization of parallel cable robot has proven to be a solution where axial misalignment is no longer an issue for the rehabilitation process [3].

2.2. Suspended Parallel Cable Robot in Rehabilitation

Suspended cable robots has been used in different areas such as Construction, Haptics, Giant Telescope Maintenance, 3D printing, and rehabilitation [16]–[19]. Studies has shown that the suspended parallel cable robot does not suffer from misalignment issue between human joints [3]. Some examples of previous utilization of cable robots in rehabilitation can be seen in the work of Alamdari *et al.* [20] in Figure 11, Nunes *et al.* [21] in Figure 12, Ennaiem *et al.* [22] in Figure 13.

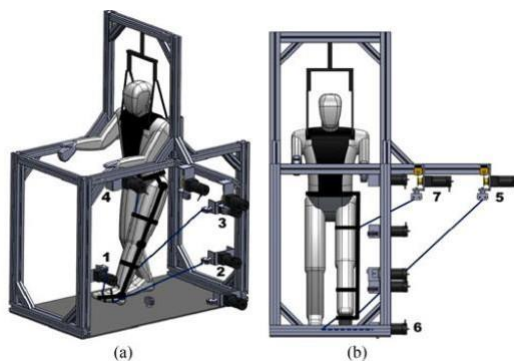


Figure 11: Cable driven rehabilitation robot for legs [20]

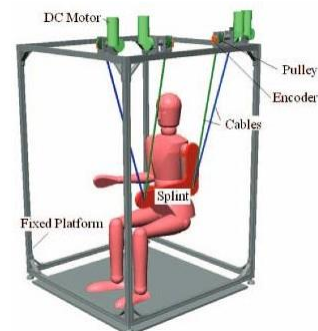


Figure 12: Cable-driven rehabilitation robot for arm [21]



Figure 13: A reconfigurable cable driven robot [22]

To the extent of the author's knowledge, there is no fully developed system for human head-neck rehabilitation robot that utilizes Cable-Driven Parallel Manipulator (CDPM); hence, this research would aim to study CDPM in head-neck rehabilitation.

2.3. Cable Driven Parallel Manipulators

CDPM can be divided into 6 categories (Figure 14) based on the degrees of freedom

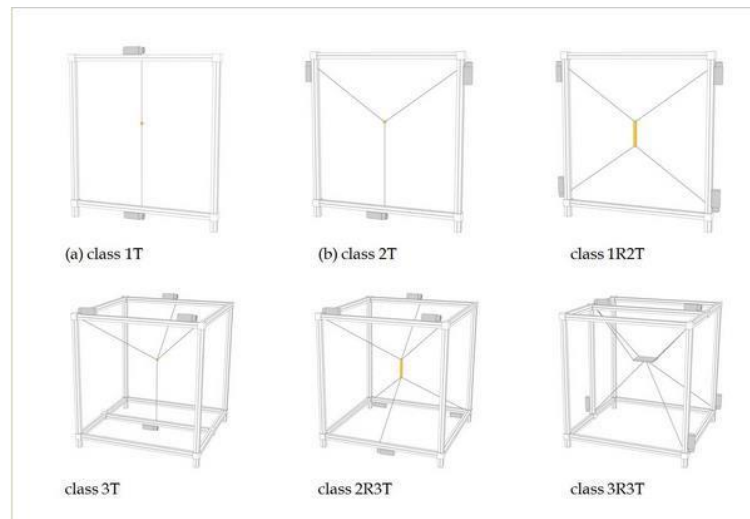


Figure 14: Types of CDPM based on degrees of freedom [23]

they provide in fully-constraint situation, that is, 1T, 2T, 1R2T, 3T, 2R3T, 3R3T, where R stands for rotational, and T stands for translational movements [23]. The modelling of CDPM is analogous to Stewart platform (Figure 15) with two major differences. First, links of the robot have unilateral constraints, i.e. the cable can only be in tension. Second, linkages lengths can be adjusted depending on length of the cable that is used for their task. Noted that one major complication with suspended cable robots is collision of the different cables during operation, which must be avoided [23].



Figure 15: Stewart parallel robot [23]

Kumar *et al.* developed a MATLAB command to study a 4 cable Static Feasible Workspace excluding control issues in their studies [24]. Gagliardini *et al.* developed a mathematical modelling, which describes the wrench feasible workspace and the dynamic feasible workspace [25]. Paty *et al.* extended modelling of cable robots to consider both cable elasticity and pulley kinematic [26].

Alp and Agrawal designed a Lyapunov based control system for controlling the

trajectory of the cable robot [27]. Mersi *et al.* developed a PID control system, which data of the cable length and an accelerometer are infused to give a better control performance [28]. Khalilpour *et al.* introduced a wave-based control to have accurate tracking and reduce vibration in cables [29]. Hosseini *et al.* designed an adaptive fast terminal sliding mode control for his project [30]. In all the control design, modeling of the system and unilateral properties of the cable seems to be the challenging part of the design.

Chapter 3. Design and Modelling

To develop a cable robot suited for the biomedical application, first all the constraints and limitations imposed by the biomedical application must be considered before designing of the robot. Then, the suitable robot with must be selected and resized according to the need of the robot. Finally, the model should be optimized for better performance of the system. This chapter will discuss all the key points in details.

3.1. Design of Cable Robot Biomedical

The accurate method of head-neck motion can be represented by a six degrees of freedom serial mechanism. The movement of the head-neck muscles are limited both by musoskeletal system and nervous system as well. The skeletal system responsible for head-neck movement is a part of a spine, which is also referred as Cervical Spine [31]. Many of treatments for head-neck movement defects are treated with a method called Cervical spine manipulation (CSM). Certain male-practices in CSM might result in occurrence of serious injuries in human body. Therefore, it is necessary to study the range of motion and stress tolerances of human body before performing any CSM.

While muscles are responsible for activating the set of motions in head-neck movement, the dominance of skeletal system has prominent role in determining the range of head-neck motion. Cervical Spine consists of 7 vertebrae, each denoted by the letter ‘C’ followed by a number, which starts at 1 in area close to skull, and it will be increased more as it will go far. C1, also known as Atlas, and C2, known as axis, are the dominant cervical vertebrae in head rotation, in such a way that translational movement of minimal [32]. To determine the range of head-neck motion, two different studies, namely active range of motion and passive range of motion are performed in ample of researches[33]–[35]. In active range of motion the human subjects have voluntary movement of head-neck, while in the passive range of motion the movement is acquired by an external force to human subject [35]. In a study performed by Moreno et al., (Table 1) the active and passive range of motion of 24 of human subjects has been measured in 3 different sessions as shown in figure [35].

Table 1: Head-neck range of motion [35]

Type of motion	Passive Range-of-Motion (deg)	Active Range-of-Motion (deg)
Full rotation	155.83	155.83
Lateral movement	39.54	40.42
Cervical Flexion/Extension	123.98	120.55

The permissible moments applied to for movement of head-neck musculoskeletal movement are studied in a separate study in different planes (Figure 16). In series of studies, the data regarding the corresponding moment for attaining required angle of head-neck has been measured as shown in Figure 17 & Figure 18. To design a robot capable of performing rehabilitation, the actuator should be capable of handling the forces required for rehabilitation process.

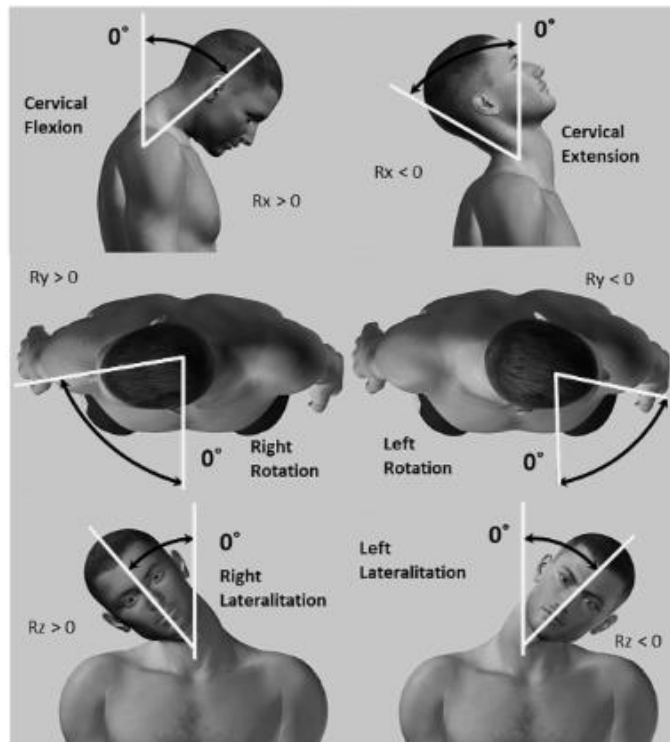


Figure 16: Type of human movement[35]

The permissible moments applied to for movement of head-neck musculoskeletal movement are studied in a separate study. In series of studies, the data regarding the corresponding moment for attaining required angle of head-neck has been measured as shown in Figure 17 & Figure 18. To design a robot capable of performing rehabilitation, the actuator should be capable of handling the forces required for rehabilitation process.

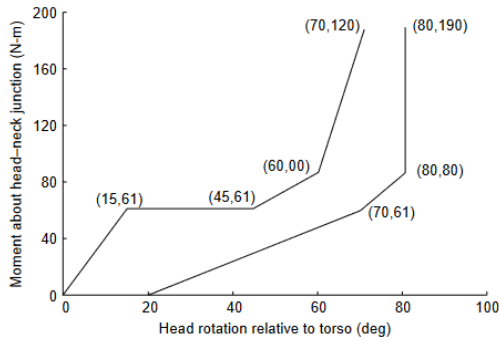


Figure 17: Neck flexion [36]

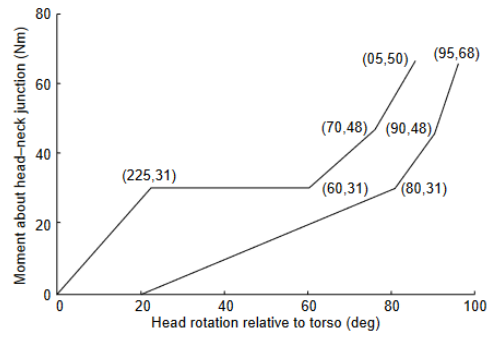


Figure 18: Neck extension [36]

3.2. Cable Mechanism

The cables used for the experiments should withstand the forces applied on the ends without any plastic deformation. Also, it is important at the place where the direction of the pulley's changing, what type of mechanisms is being used. For instance, According to a review generally there are four outlet mechanism as shown in Figure 19: eyelet type; single pulley type, double pulley type, multipulley type [37]. Eyelet exists provide a simpler solution in terms of modelling; nonetheless, cables passing through eyelet will reduce the lifetime of the cables due to high friction which wears the cables [38]. Using pulleys will allow a smoother motion yet introduces inaccuracies in modelling, which can be improved.

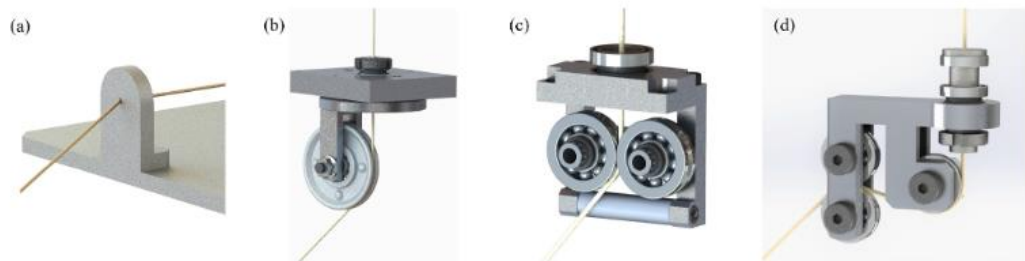


Figure 19: Outlets: (a) eyelet, (b) single-pulley, (c) double-pulley, (d) multi-pulley [37].

Cable mechanisms (Figure 20) undergo a constraint, namely, unilateral condition. Unilateral constraint in mechanisms is type of constraints that will allow a member to exert force on other members or object only in one direction, which in the case of cable-based mechanisms, is only when cables are under tension.

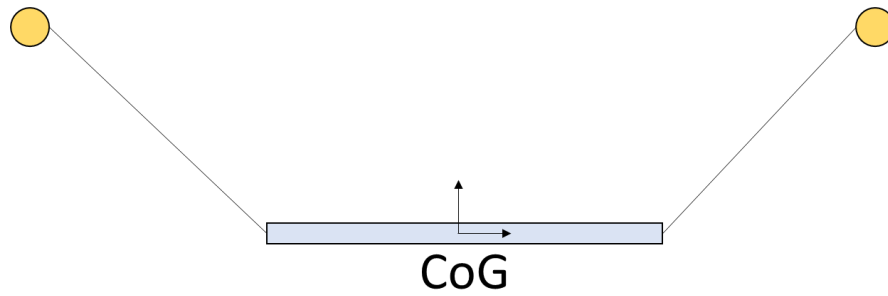


Figure 20: Cable robot rehabilitation

Due to this unilateral condition, the degrees of freedom N are subjected to the number of cables m attached to the platform. The following formula can be established.

$$N = M - 1 \quad (1)$$

N : Degrees of Freedom

M : Number of Cables

Important note on equation (1) does not limit the movement in other direction due to slack in cables when they are not tension. Movement in other direction in presence of external forces, where the cables are not under-tension is possible, which is referred as under-actuated system. To have a better control in a certain workspace, sometimes additional cable is added to the system, where for the targeted degrees of freedom is considered as over-constrained system. Therefore, one may deduce 6 type of cable robot, as in Table 2:

Table 2: Type of cable robots

Class	Type of Motion	Degrees of Freedom
1-Translational (1-T)	Linear motion	1
2-Translational (2-T)	Planar motion	2
1-Rotational-2T (1R2T)	Planar motion	2
3T	Spatial motion	3
2R3T	Spatial motion	3
3R3T	Spatial motion	3

The aim of this thesis project is to control head-neck movement in a plane; hence, 1R2T cable robot is selected for the purpose of head-neck rehabilitation.

Since 1R2T cable robot has three degrees of freedom, according to equation (1) 4 cables are required to perform the necessary action under cable robot. The cables are arranged in a rectangular arrangement (Figure 21).

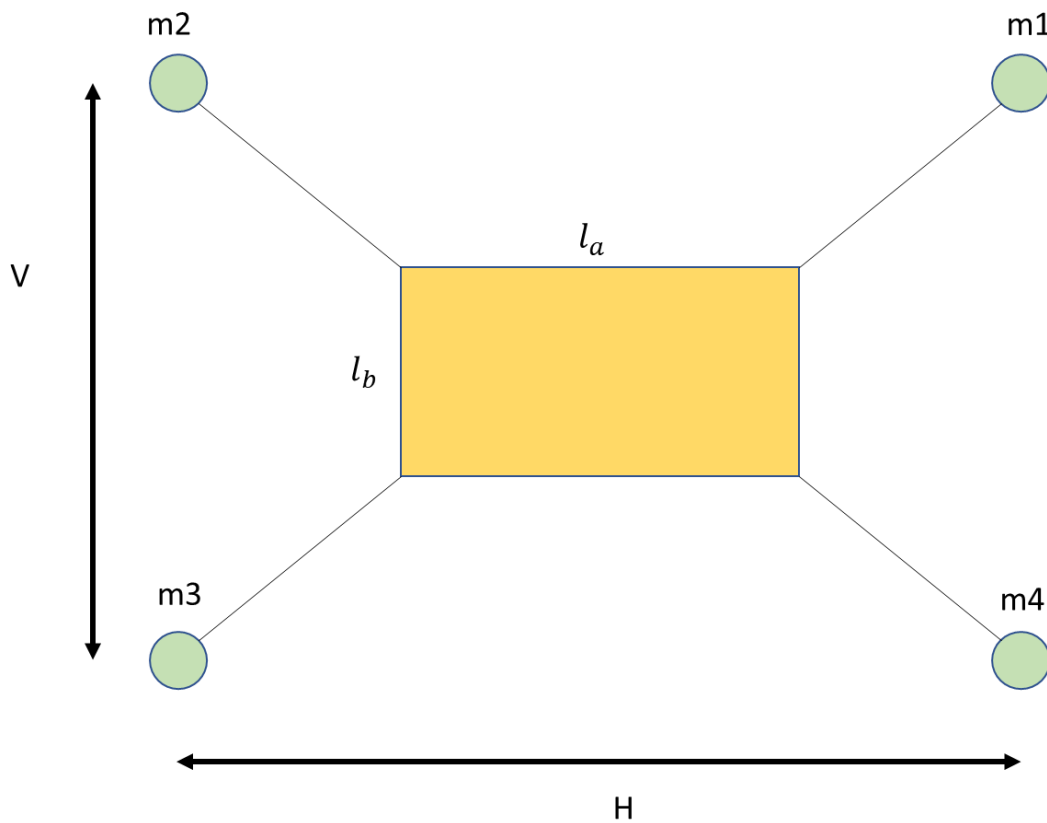


Figure 21: 1R2T cable robot without intermediate stage

Cables are attached to winch or pulley mechanism on one end, and on another end it is attached to the end effector. To facilitate the angular movement of cables, in intermediate stage, an idler pulley would be used to allow cables to have rotation and have more accuracy (Figure 22). Therefore, the model would be enhanced accordingly.

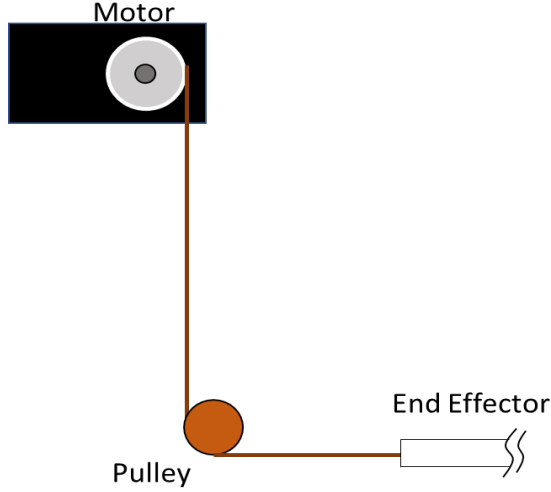


Figure 22: Motor pulley end effector

Assuming that there is pulley that can rotate in xy-plane, now we can construct geometric model accordingly.

3.3. Inverse Kinematic Model

To construct the inverse kinematic model, the desired coordinate system should be selected (Figure 23). In Inverse Kinematic Model (IKM), a global coordinate would be selected on the earthed link, and local coordinate would be selected on the end effector position. Then, the system would be represented by vectors, which captures the general physics of the mechanism. In Figure 23 there are two paths of vectors; one from global coordinate system to Center-of-Gravity of platform, and then to point w; the other path from global coordinate system origin to motor, and then single pulley, and then to anchor point at w. the direct path to the platform is constructed for ease of modeling when global coordinate system is at the camera or observer location.

$$\vec{l}_{op} + \overrightarrow{PW} - \vec{c} - \vec{b} - \vec{a} = 0 \quad (2)$$

The parameter of interest is \vec{c} , and the location of global system is arbitrary, preferably at the origin place of platform, or at the location of cameras. It is therefore required that.

$$\vec{c} = \vec{l}_{op} + \overrightarrow{PW} - \vec{b} - \vec{a} \quad (3)$$

The local coordinate system P in Center-of-Gravity (CoG) of platform in Figure 23 is defined, so that the anchor point, where cables meet the platform, can be defined at point w. to find the exact location of the point w in the global coordinate system, one

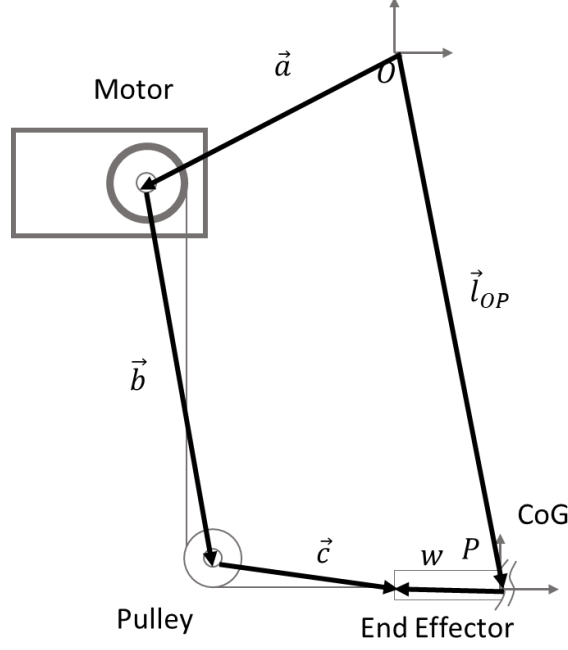


Figure 23: Vector Representation of the system

must define the Euler rotation matrix R_{zyx} as in:

$$R_z = \begin{bmatrix} \cos(\theta) & -\sin(\theta) & 0 \\ \sin(\theta) & \cos(\theta) & 0 \\ 0 & 0 & 1 \end{bmatrix} \quad R_y = \begin{bmatrix} \cos(\theta) & 0 & \sin(\theta) \\ 0 & 1 & 0 \\ -\sin(\theta) & 0 & \cos(\theta) \end{bmatrix} \quad (4)$$

$$R_z = \begin{bmatrix} 1 & 0 & 0 \\ 0 & \cos(\theta) & -\sin(\theta) \\ 0 & \sin(\theta) & \cos(\theta) \end{bmatrix} \rightarrow R_{zyx} = R_z R_y R_x$$

Hence, the equation (3) can be written as:

$$\vec{c} = \vec{l}_{op} + R_{zyx}w - \vec{b} - \vec{a} \quad (5)$$

Notice that the vector \vec{c} is output to the inverse kinematic model, and the input is vector \vec{l}_{op} and matrix R_{zyx} are the input of the equation. If we assume that the magnitude of the vector \vec{c} is depended on angle of motor with rotational angle of θ and radius r , we then have:

$$r\theta = |\vec{l}_{op} + R_{zyx}w - \vec{b} - \vec{a}| \quad (6)$$

Notice that the angle of θ is corresponding to a point depending on the origin.

Therefore, to compensate for effect of change in origin, initial angle θ_0 is introduced

$$r(\theta + \theta_0) = |\vec{l}_{op} + R_{zyx}w - \vec{b} - \vec{a}| \quad (7)$$

Thus, the desired angle θ can be calculated through the equation (8)

$$\theta = \frac{|\vec{l}_{op} + R_{zyx}w - \vec{b} - \vec{a}|}{r} - \theta_0 \quad (8)$$

3.4. Rotation to Planar Movement Mapping

For the purpose of rehabilitation, the movement of the head, which is in form of a rotation, should be mapped to a certain planar path due to the planar movement of the robot. A mathematical approach to solve the issue is by creating a conical section between the head pivot point and the plane (Figure 24), in which the robot moves as shown in Figure 24.

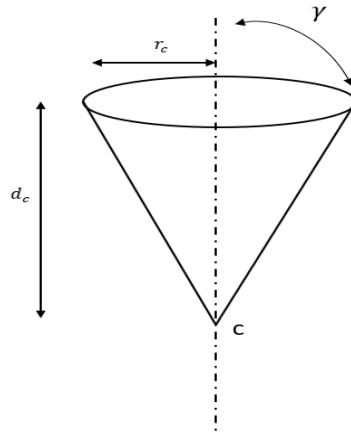


Figure 24: Conical section corresponding for certain angle movement

The corresponding rotational angle γ or the distance r_c can be obtained through the following:

$$\tan(\gamma) = \frac{r_c}{d_c}$$

r_cdistance from neutral point of head in the robot plane (9)

d_c Vertical distance between plane of motion and pivot point of head

γRotational angle of head-neck motion

Hence, we have:

$$\gamma = \text{atan}\left(\frac{r_c}{d_c}\right) \quad (10)$$

and through vector analysis, of a selected point on a circle, one can describe how much of this angle contributes to flexion/extension, and how much to lateral rotation.

Chapter 4. Experiment Methodology

To verify the mathematical modelling established in the chapter 3, an experimental setup has been developed to measure the values of input and output of the proposed system. This chapter discuss the setup made for verification of model followed by study of 11 cases of path movement using independent joint control. A PID controller scheme has been used within the servo motors to control the position of the motor based on the feedback loop received from the encoder of the servos.

$$u = k_p e + k_i \int e dt + k_d \frac{de}{dt}$$

u : control signal (V)
 e : error signal (deg) (11)
 k_p : propotional gain
 k_i : integral gain
 k_d : differential gain

The performance of the system has been measured through various indices in this study. One of the important indices that are used to measure the system performance is Integral Square Error (ISE), Integral Absolute Error (IAE), Integral Time Absolute Error (ITAE). ISE tends to highlight stead large errors, ITAE shows the transient error behaviour of the system, and IAE does not add any weight to steady or transient error.

$$ISE = \int e dt \quad (12)$$

$$IAE = \int |e| dt \quad (13)$$

$$ITAE = \int t|e| dt \quad (14)$$

4.1. Experimental Setup

The cable robot designed for this experiment consists of 4 dynamixel MX64-AT servo motor; four pulley drum, that is assembled on the motors; four idler pulleys, and a platform made of PLA as shown in Figure 26. The cable used for this experiment is a made of nylon and fluorocarbon, and capable of handling 130 N force before breaking. The motors used for this experiment have the parameters in Table 3 and performance chart in Figure 25:

Table 3: MX64-AT motor parameters [39]

Dynamixel MX64-AT	
No Load Speed	63 rev/min
Motor	Coreless
Position sensor resolution	0.088°
Stall Torque	6.0 N.m
Encoder Bit	12 bit
Backlash	0.33°

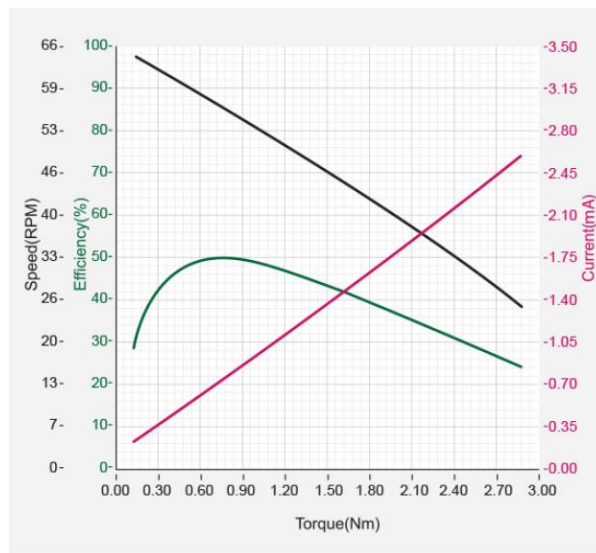


Figure 25: Performance chart of MX64-at graph [39]

Based on the information of Figure 18, the neck flexion torque requirement at passive range of motion will reach to 6 N.m. Since four of these motors are used to move the head-neck motion, the torque requirement for this experiment is satisfied. A rectangular platform has been 3D printed using PLA filament, to be used as end-effector of the robot as in Figure 26.

The structure used for the cable robot is made of T-Slotted aluminum 6061 alloy with 20x20 mm profile. And before construction of the actual robot, 3D model of the robot has been made using Solidworks 2021 Academic version to visualize the design

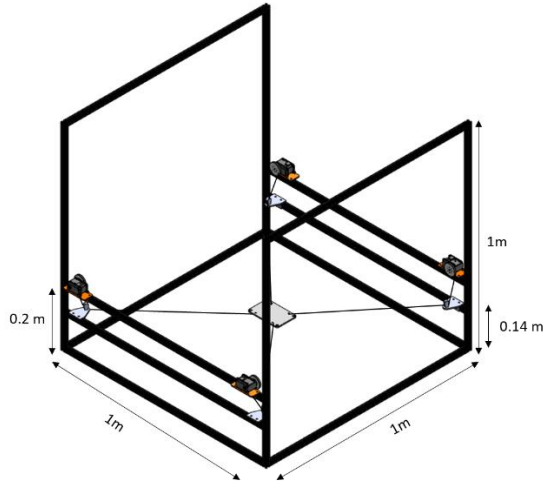


Figure 26: Robot structure

The pulleys assembled on the motors are single threaded drum with inner diameter of 4.5 cm (Figure 27 & 28). The actual setup is shown in Figure 29.

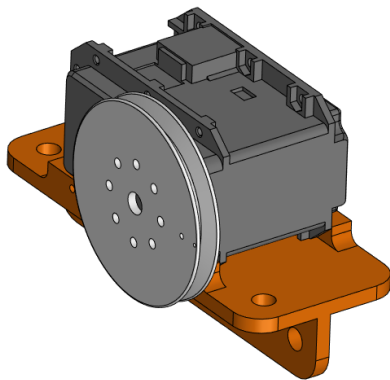


Figure 27: Motor model with pulley

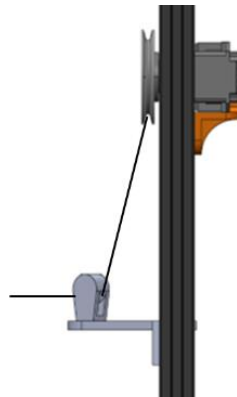
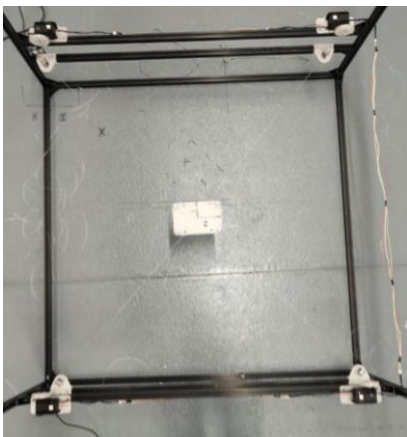
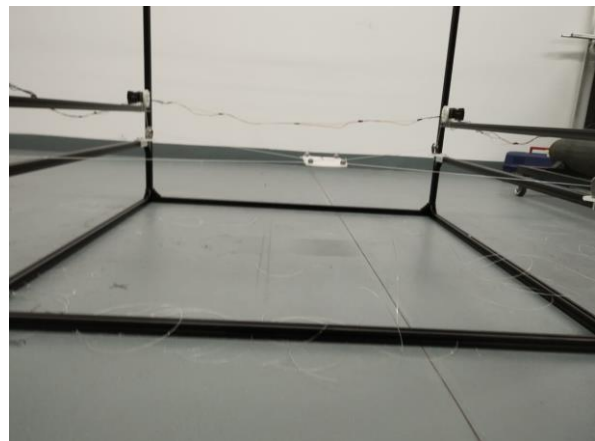


Figure 28: Motor pulley and idler pulley



(a)



(b)

Figure 29: Parallel cable robot: (a) Top view, (b) side view

The motors communicating with computer and among themselves through RS485/TTL Half Duplex Asynchronous Serial Communication with 8bit, 1stop, No Parity. Motors communicate at 57600 bps and they are attached is shown in Figure 30. Microcontroller used for the MX64-AT motor is ST CORTEX-M3 (ST32F103C8 @ 72MHZ,32BIT), and the motor used for this experiment is maxon DC motor.

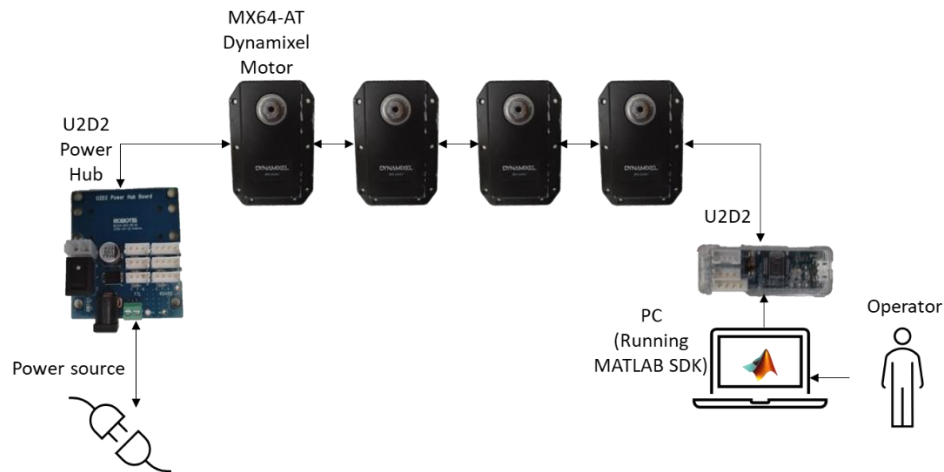


Figure 30: Motor communication network with PC

The dimensions of the platform and idler pulleys are given as Table 4 for Figure 31.

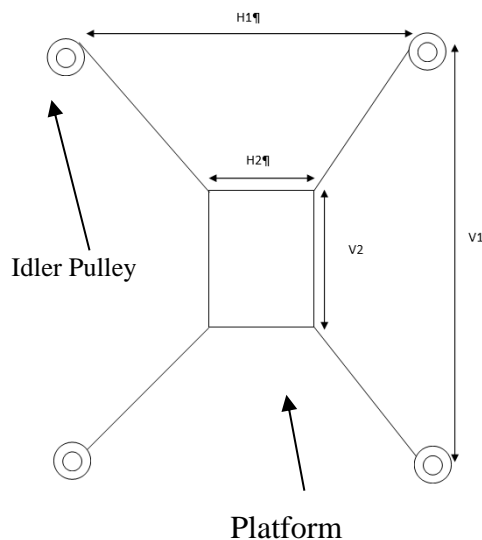


Figure 31: Platform dimensions

Table 4: Planar parameter of the cable robot

Parameter	Unit
V1	0.86 m
H1	0.94 m
V2	0.08 m
H2	0.08 m

The measurements of the cable robot in the spatial space have been done through Opti-Track setup (Figure 32), which consists of 12 cameras (as in Figure 32). 4 markers attached to the places where idler pulleys are placed, and 4 markers attached to the platform itself. By creating two objects in the Opti-Track, one platform and another the

frame, the setup has been defined within a confined space. The Opti-Track has been recalibrated before operation and the following set of parameters has been obtained. Notice that the mean value error in the calibration is 0.453 mm (Figure 33).

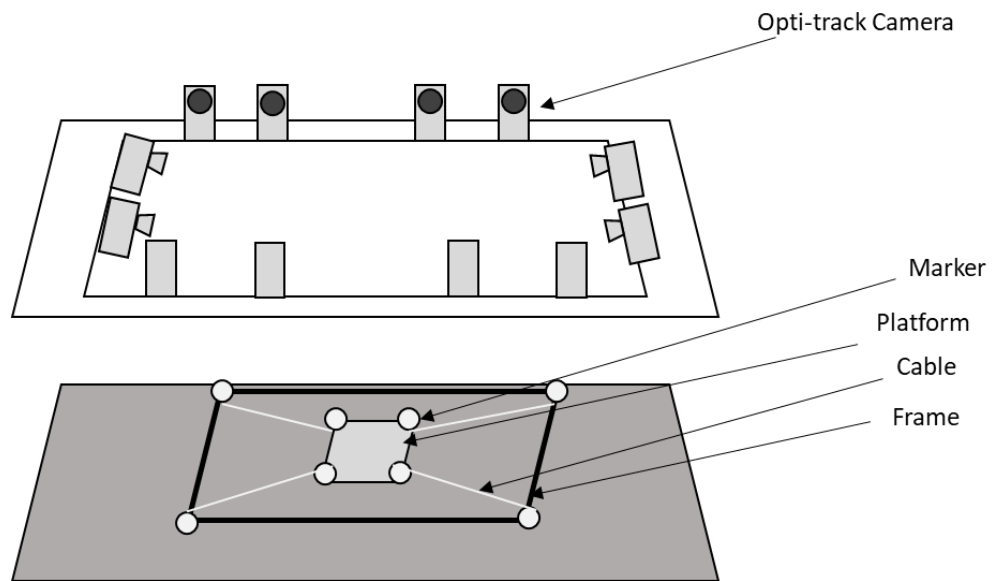


Figure 32: Opti track configuration

The global reference in this experiment is where 'Frame' is defined, and the platform coordinate system is where 'Platform' is defined in the Opti-track. The performing transformation between these two objects, the global place of the platform has been defined.

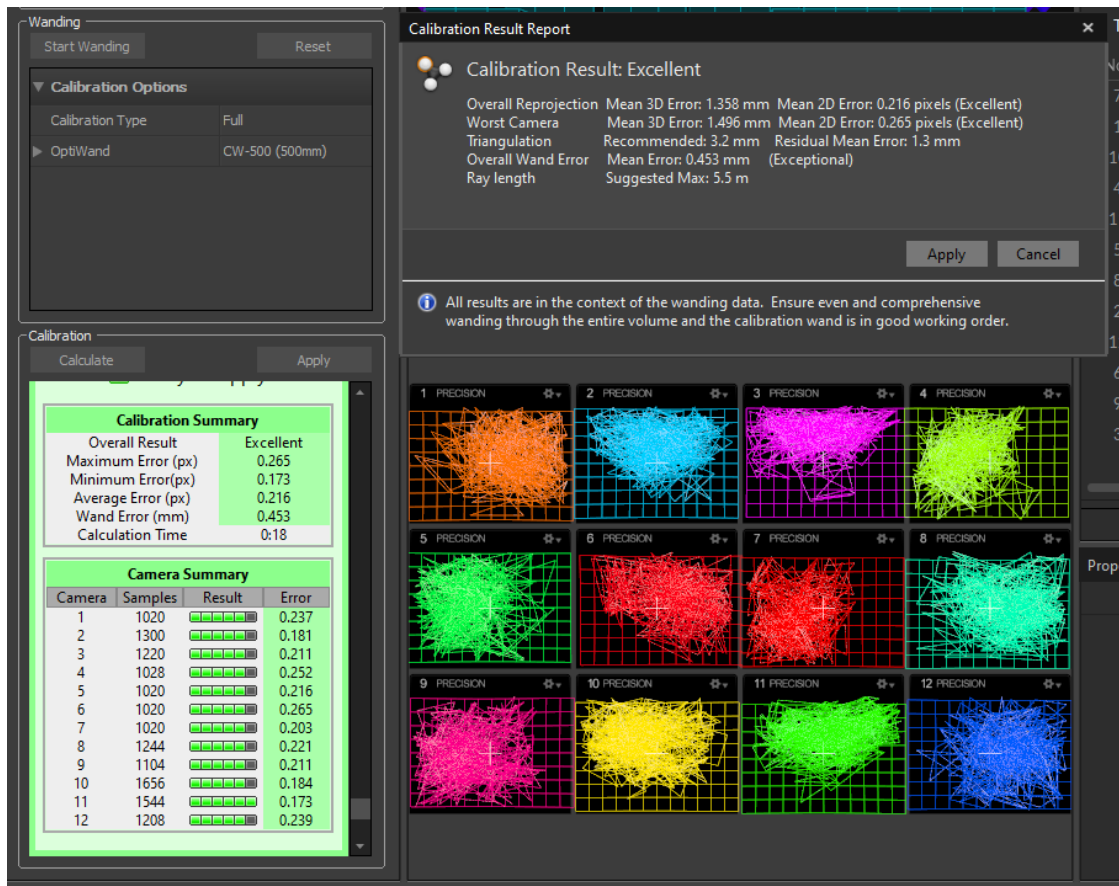


Figure 33: Opti-Track calibration results

The servo motors used in this experiment are capable of tracking a given angle using an in-built Proportional-Integral-Derivate (PID) controller (Figure 34). The values of these PID controller can be changed and tuned depending on the transient and steady state response needed by the designer. In this experiment the gain used for PID controller is shown in the table 5:

Table 5: PID gains

Parameters	Value
K_P	240
K_I	48.83
K_D	2.4

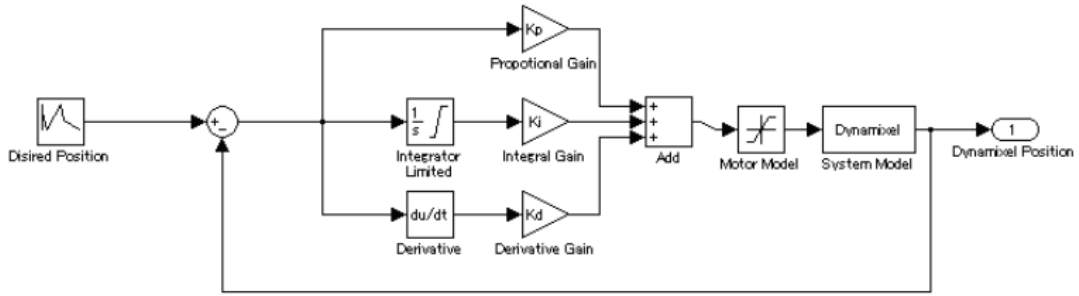


Figure 34: Dynamixel PID controller [39]

4.2. Model Validation and Error Analysis

To understand the inaccuracies of the model, several case studies has been conducted, so that the errors of the model can be evaluated by using different parameters and measure the repeatability of the results. The Table 6 summarizes all the cases and experimental parameters that has been studied in this research.

Table 6: Summary of cases studied

Case No.	Shape	Trials/Cases	Seed Number	Dimensions	Trapezoidal Movement Velocity	Trapezoidal Movement Acceleration
1	y-Infinite	3	400	20x20 cm^2	229 rpm	37.45 rad/s^2
2	x-infinite	3	400	20x20 cm^2	229 rpm	37.45 rad/s^2
3	x-infinite	3	400	20x20 cm^2	22.9 rpm	3.745 rad/s^2
4	x-infinite	3	400	20x20 cm^2	Impulse	Impulse
5	x-infinite	3	400	15x20 cm^2	229 rpm	37.45 rad/s^2
6	x-infinite	3	400	10x20 cm^2	229 rpm	37.45 rad/s^2
7	x-infinite	3	200	20x20 cm^2	229 rpm	37.45 rad/s^2
8	x-infinite	3	100	20x20 cm^2	229 rpm	37.45 rad/s^2
9	Circle	2	50	20x20 cm^2 30x30 cm^2	229 rpm	37.45 rad/s^2
10	Ovel	3	50	20x20 cm^2	229 rpm	37.45 rad/s^2
11	Rectangle	3	100	20x20 cm^2	229 rpm	37.45 rad/s^2

4.2.1. Case 1

In this experiment, the number of the seeds is 400 and a slow trapezoidal movement between via point has been selected (229-rpm velocity, 37.45 rad/s^2 acceleration), and the trapezoidal trajectory between each point has been selected. As shown in Figure 35, the robot follows the path almost in all directions. It was noticed that the robot

follows the desired angular position a certain shift in the graph for all three cases, which shows that the repetition of the experiment does not affect the result of the experiment in terms of motor angle (Figure 36). This can be explained by the fact that motor position is controlled by a close-loop PID controller.

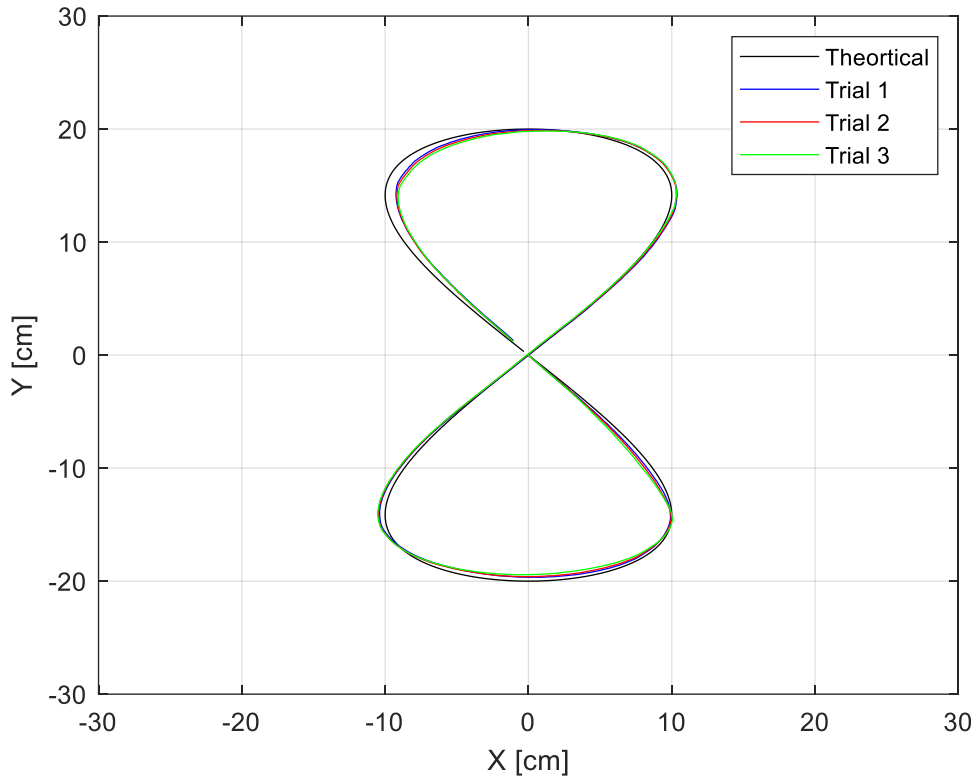


Figure 35: Infinity along y trial planar movement case 1

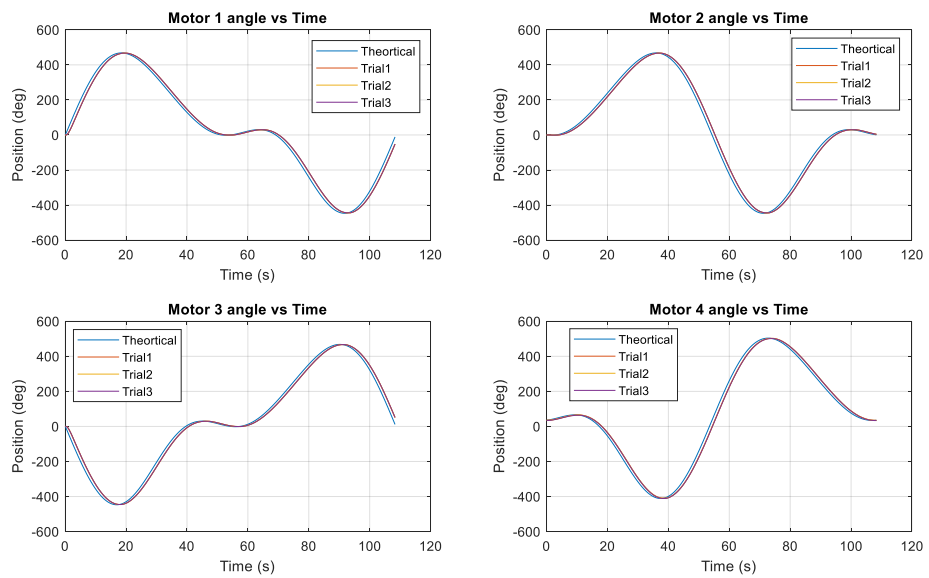


Figure 36: Motor angular position trajectory case 1

The speed of the motor in presence of the trapezoidal movement between the via points shows a relatively smooth transition, also the graph of the three trials coincides with each other (Figure 37), which also supports the fact that the experimental results are repeatable.

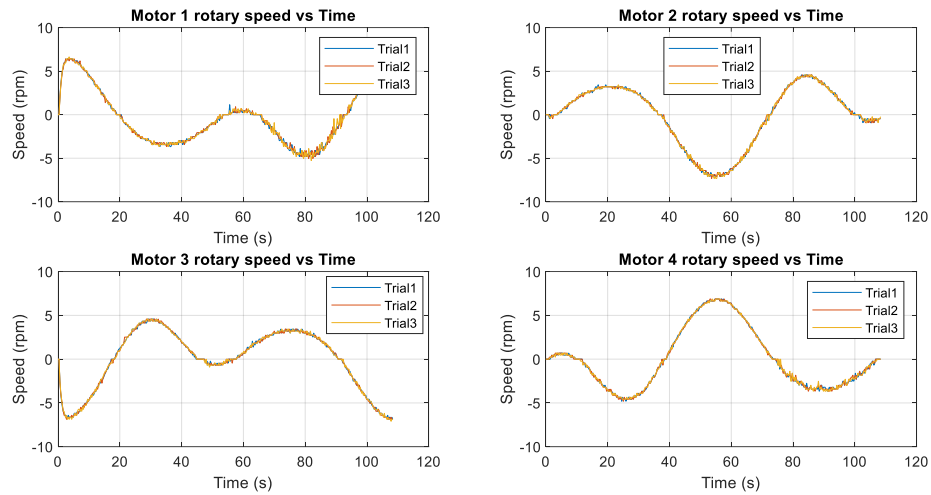


Figure 37: Rotary speed vs time for case 1

As for the current measurements, it has been observed that the motor current increases in additional trials. One explanation of this phenomenon is that since there is an assumption that the platform always starts from the middle of the platform, any inaccuracies due to this assumption will lead to disturbance of the system in terms of the torque, which yields to drawing higher current (Figure 38).

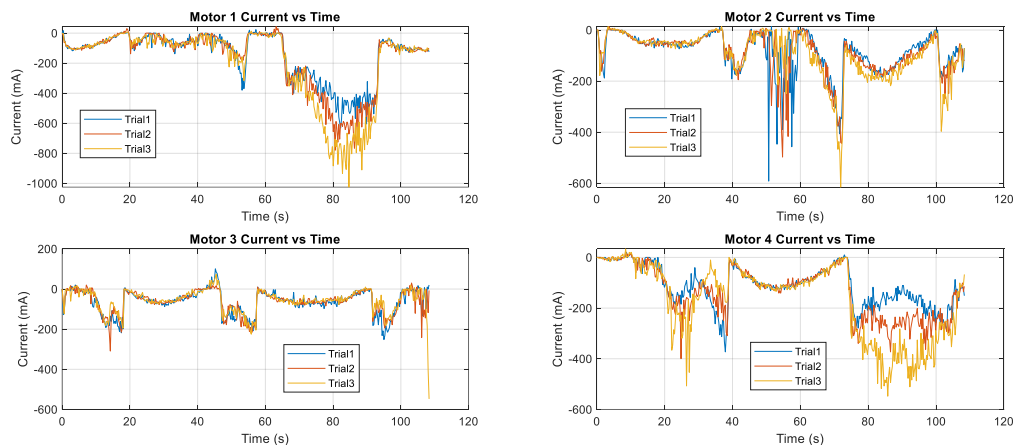


Figure 38: Motor current measurements for the case 1

In terms of the error, it is evident that the error in the x and y plane is systematic. Which indicates the fact that some of the modeling parameters are needed to be adjusted, while in the z axis, it has been observed that the error increases in each trial,

which is a random error possibly due to the need of recalibration of the platform position in each trial (Figure 39-42).

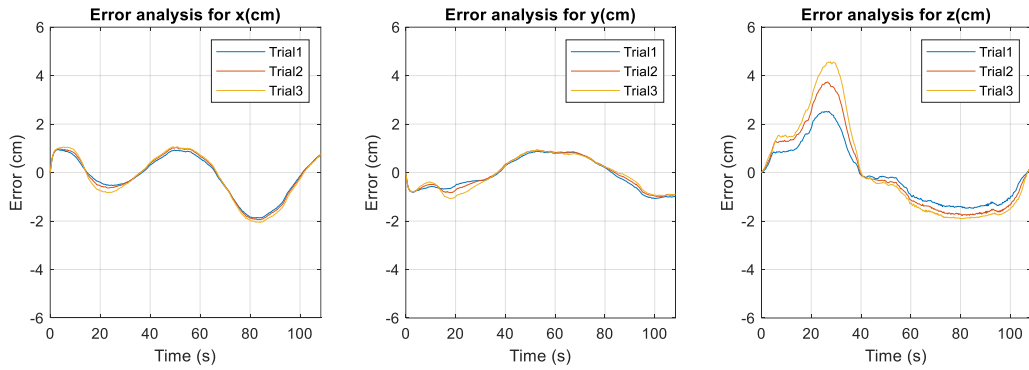


Figure 39: Error measurements of case 1

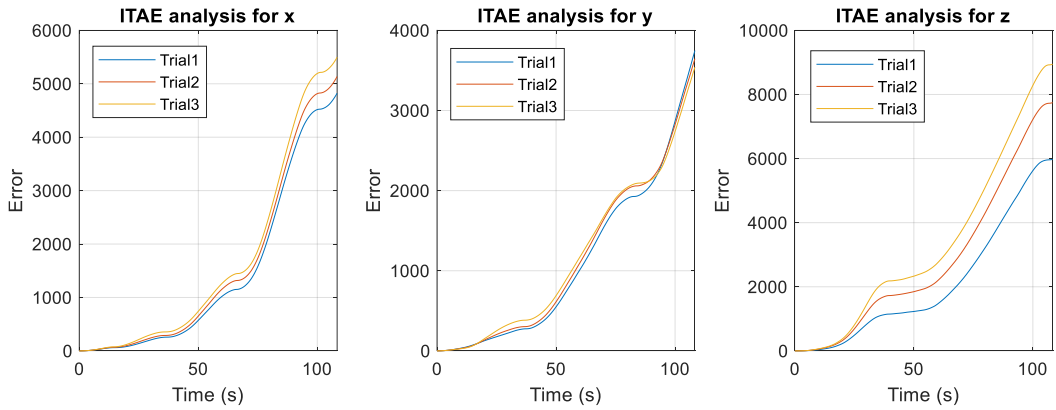


Figure 40: ITAE errors generated in case 1

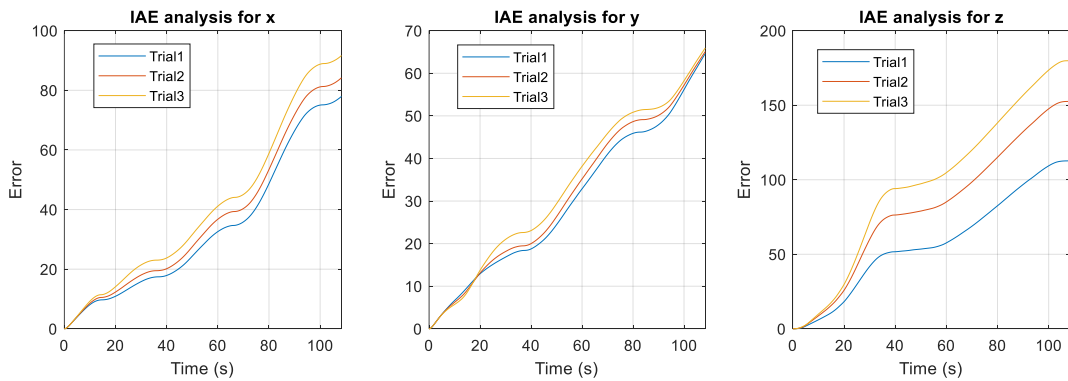


Figure 41: IAE error generated in case 1

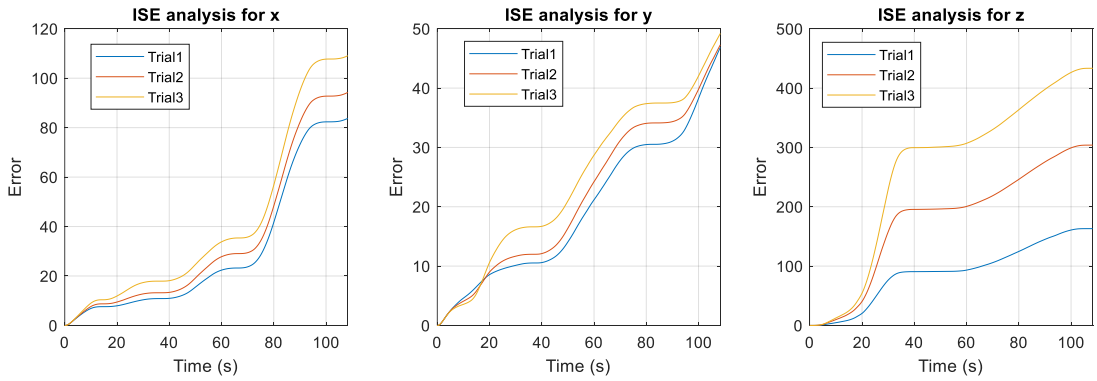


Figure 42: ISE error analysis in case 1

Error performance analysis suggests that the modeling is prominent source of error in x and y axis, while in z axis, the error will increase in more trials.

4.2.2. Case 2

In his experiment (Figure 43), the number of the seeds is 400 and a fast trapezoidal movement between via-point has been selected (229-rpm velocity, 37.45rad/s^2 acceleration) and the movement is across the x. The values of the position in the case 2 follows the desired point obtained by the inverse kinematic model. There is a mild shift between the desired point and experimental data, which is expected due to the use of trapezoidal profile between the points. The motion of the platform during the experiment is smooth with exception of the areas, where speed is held at a constant rate. In overall, there is no impact expected by the smooth motion of the platform. The current consumed during the experimentation does not follow a constant path in certain areas, which is an indication of a disturbance in the system as the number of the trials progress. This can also be attributed to home positioning same as the case 1. In the error analysis of the case2, it is noticeable that the error in x axis and y axis relatively increases as number of trials increases. The error indicators show that that the transient error has more dominant effect on the experiments, also the third trial has more error, which indicates that truncation error will be introduced in the system without performing calibration in the system for each trial.

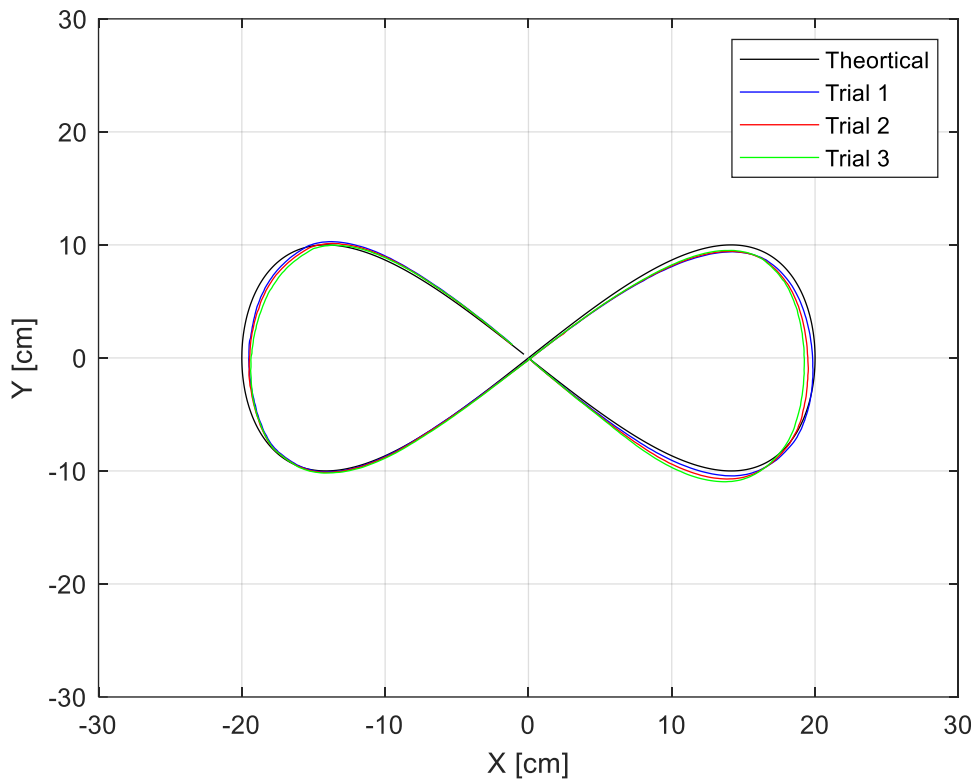


Figure 43: Infinity along x trial planar movement case 2

4.2.3. Case 3

In this case (Figure 44), a slower motion of trapezoidal movement has been selected (22.9-rpm velocity, 37.45rad/s^2 acceleration) to study the effects of path motion on the error generated on the system. In this case, it has been established that, at the slower rate, motors follow the desired path with a minimal shift, which is expected to produce more accurate results compared to case 1 and case 2. The motion is relatively smoother in case 3, the ripples are smaller compared to case 1 and case 2. The current profile would exhibit more chaotic behavior as the number of trials increases. Nonetheless, this chaotic behavior is more of a small ripple than major changes. The error in positioning of the system will increase as the number of the trials increases. One important factor is that since slower trapezoidal movement has been selected, the amount of the error measured by system is much lower than cases with fast speed. The performance of the system in this case is better compared to cases where the speed of the platform was higher, although the error in z axis is more persistent than another axis.

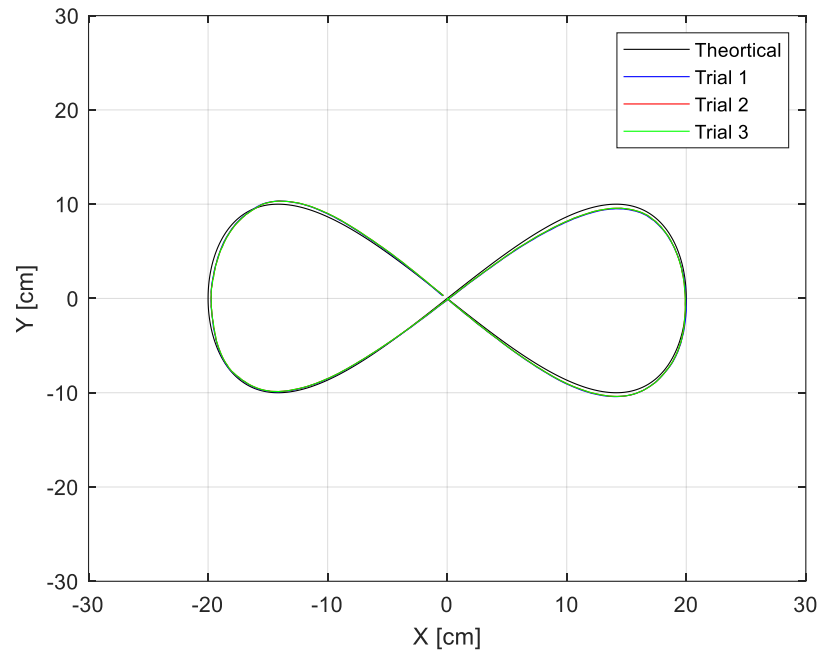


Figure 44: Infinity along x trial planar movement case 3

4.2.4. Case 4

As for the case 4 (Figure 45), a step profile has been used to move between the via points, which results in stopping at any given point to the motor before moving to the next point. The movement of the platform in this trajectory endures vibration in the system due to changes in the acceleration of the system. The profile of motor position exactly coincides with the given point to the motor, which supports the fact that the slower rise time between moving among the via points will introduce error in the results. The robot follows a less chaotic behavior in terms of the motor speed, yet presence of the ripples in the system is visible in the results taken from the motor. The current profiles in case 4 have ripples in the signals, and the ripples increases as the number of the trials increases. The reason for increment in small vibration behavior can be due to the shock introduced by sudden movement of the platform between the via points. The error signal in case 4 has a lot of ripples, which is due to the vibration of the system. Also, the quality of the movement has improved in x and y axis. Nonetheless, the error signal in the z axis endures a greater error compared to case 3.

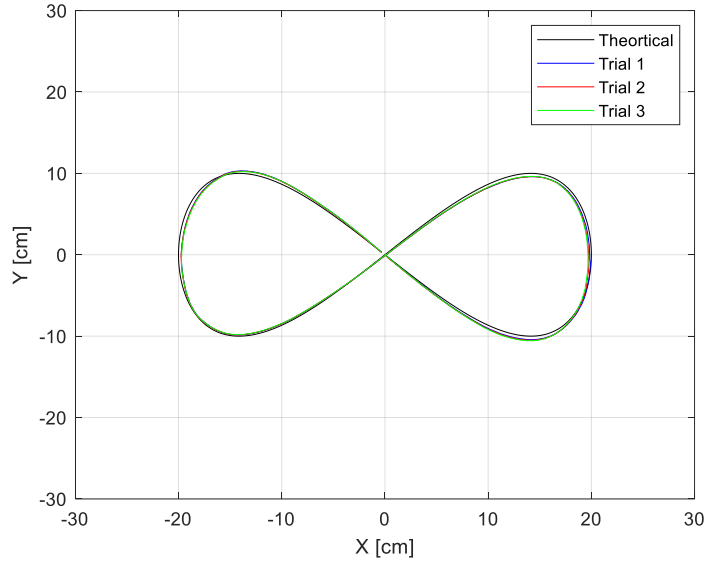


Figure 45: Infinity along x trial planar movement case 4

4.2.5. Case 5

In case 5 (Figure 46), the trapezoidal movement has been selected, (229-rpm velocity, 37.45rad/s^2 acceleration), and the infinite shape used in this profile has lower width compared to case 2, which has almost similar settings to this case. The motor profile follows the path given defined in the program, yet there is a lag in the system, but there is no significant change in behavior compared to case 2. The motor speed endures a massive ripple at the points where the average of the velocity profile is constant. Hence, it can be concluded that the lower rise time will yield to high ripples in the system. In this case, it has been shown that the smaller path will yield to more ripples in the system. Possibly due to the fact that the cables are not fully tight, and they are under the effect of gravity in the middle points. The error in the x and y axis are more systematic and hardly changes after increasing the number of trials. On the other hand, the z-axis error has a significant change of behavior as number of trials increases. The error is prominent in the z axis considering all error performance parameters. This not In addition, the error performance parameter for the y axis has been decreased considering the lowering the infinite shape size in the y axis.

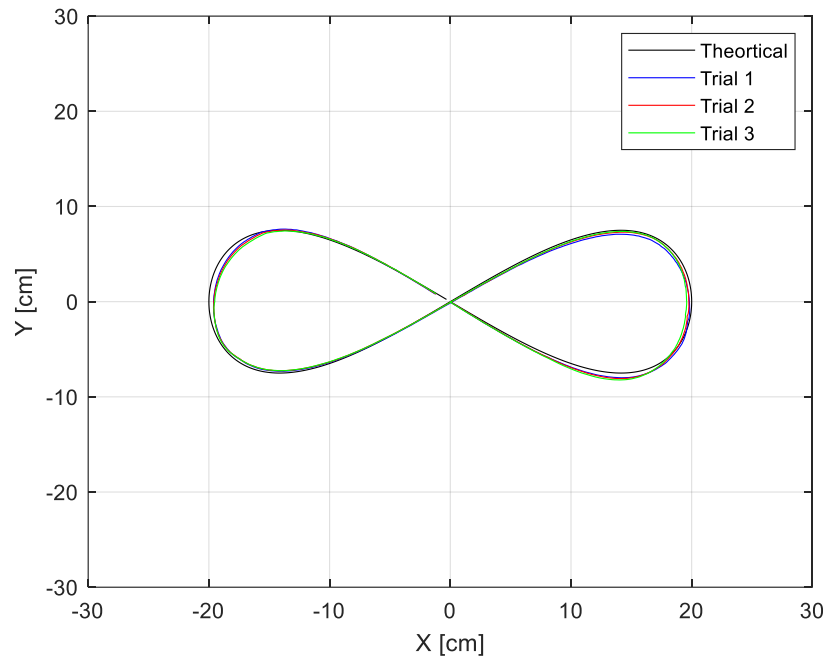


Figure 46: Infinity along x trial planar movement case 5

4.2.6. Case 6

In case 6 (Figure 47), the dimension of y axis of the infinite shape has been decreased compared to case 2 and case 5, and the trapezoidal profile has been selected for the experiment (229-rpm velocity, 37.45rad/s^2 acceleration), A certain shift in the motor profile has been observed in case 6, which can be attributed to the fact that the motor follows a trapezoidal movement between the via points. Motor 4 experiences a shift in each trial, which can be due to the backlash of the motor in each experiment. The speed profile of the system endures ripple in in each trial, but the general pattern of the motor speed remains same in all trials. The current behavior in this case is more chaotic than case 2 and case 5. Also, the repetition of results is not possible, which may indicate that the vibration of system has introduced randomness in torque exerted on the motor. The error in case 6 has almost same behavior in most of the cases. Repetition of results can be seen in all dimensions except the z axis. The error performance of the system in all the cases indicates that the trial 3 has considerable error in z axis. Hence, a certain measure of control of calibration is required while the robot is operating before it diverges any further.

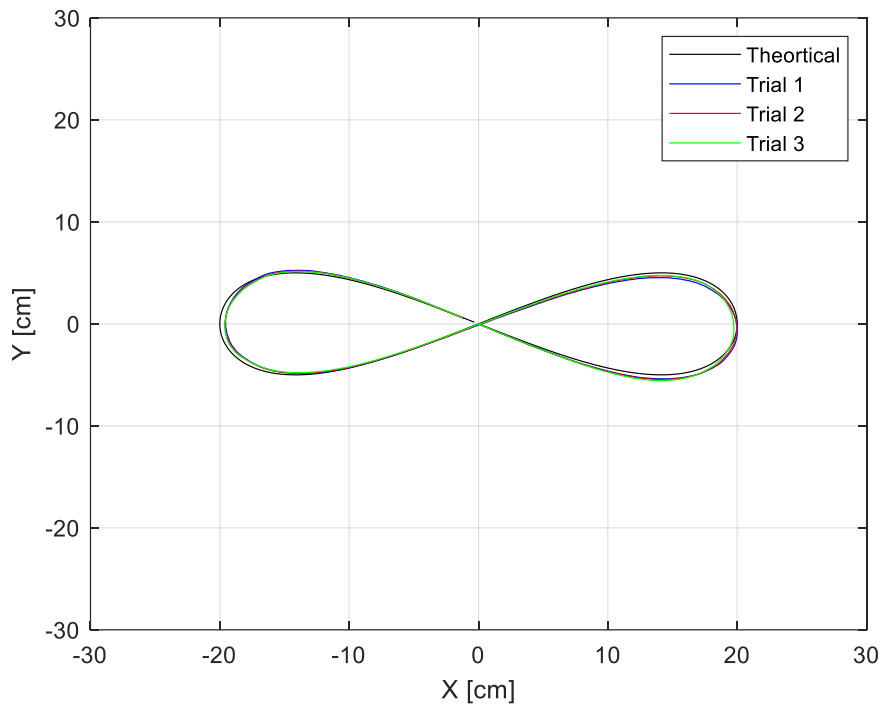


Figure 47: Path generated in case 6

4.2.7. Case 7

Case 7 (Figure 48) is special form of case 2, with only difference that instead of 400 seed point for defining the path, only 200 seed point has been used. As the result of that, the system exhibits certain chaotic path compared to the case 2. There is considerable shift in motor pattern compared to case 2, which indicates that the lesser defined points on the path will lead to more inaccuracy in motor command. The motor behavior exhibits lesser ripple compared to the case 2, and in all trails the velocity pattern is almost same. The behavior of the currents in the motors are not following a certain pattern, which indicates that the homing position of the cable robot is not accurate after each trial, which was the intension of this study. Contrary to case 2, error key indicators increase as the number of trials increases, which suggests that random error is prominent in cases with lower seeding points.

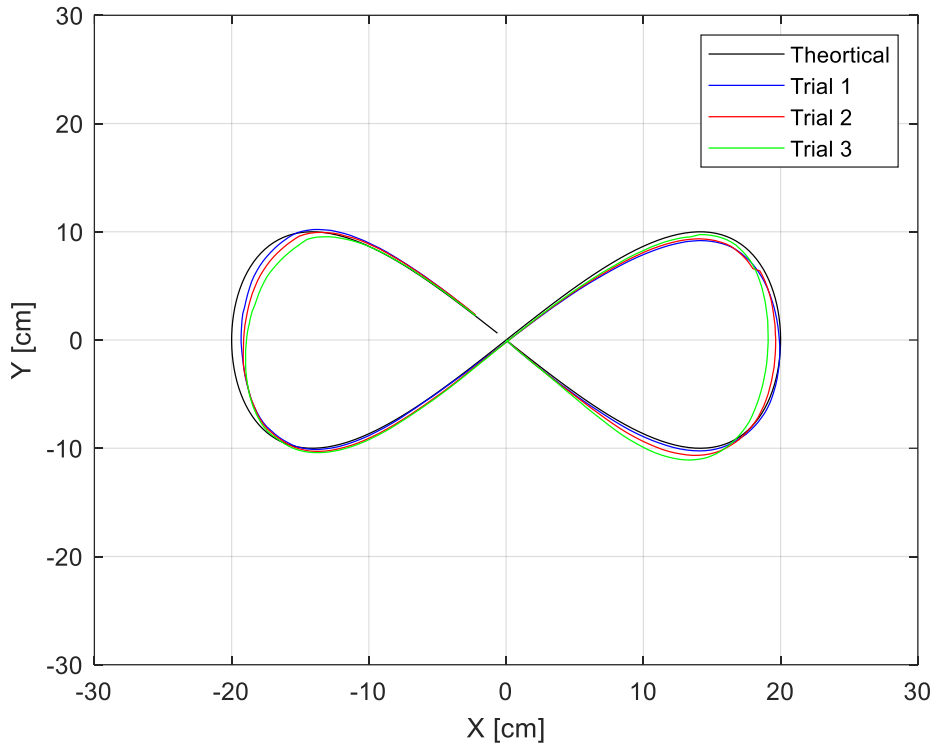


Figure 48: Path generated in case 7

4.2.8. Case 8

Case 8 (Figure 49) is special case of case 2, where the number of seeds is 100. The overall behavior of the system suggests that the system deviates from its original path as the number of trial increases, which means that the motors must be recalibrated often in a case where number of points are lower than other cases. Using lower number of seeds has proven to have major effect on shifting of the motor profile compared to the given point given to them as well as using a trapezoidal movement between the points. It the speed profile of the motor with lower number of seeds does not have ripples, and the behavior of motor is same in all trials. The behavior of the current in the motors is chaotic and no pattern can be observed, or it has drastically changed between the trials. This suggests that the external forces are more prominent with cases of lower seed, and higher error is expected compared to case 2. The error in all 3 axis is higher than case 2 and case 7. It is also shown that the pattern of error is repeatable in x and y axis, but in z is not repeatable. This indicates that there is a systematic error in the x and y axis, while in z axis other factors have influenced the behavior and caused larger error in each new trial. In this case, it is evident that the z-axis accumulation of error among trials is considerably large in comparison with all cases, and there is a considerable

systematic error in x-axis and y-axis. This indicates that for lower seeding points, motors must be calibrated.

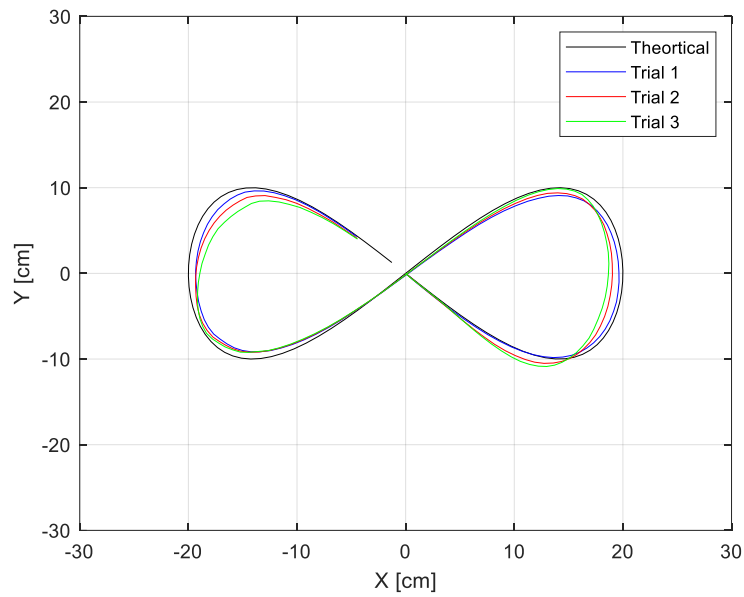


Figure 49: Robot path for the case 8

4.2.9. Case 9

In case 9 (Figure 50), a trapezoidal velocity profile has been selected (229-rpm velocity, $21,457 \text{ rev. min}^{-2}$ acceleration). Experiment 1 is a path of a circle with radius of a 20 cm, and experiment number 2 is a path of a circle with radius of 30 cm. Only 50 seed have been utilized since higher values will result in slower motion

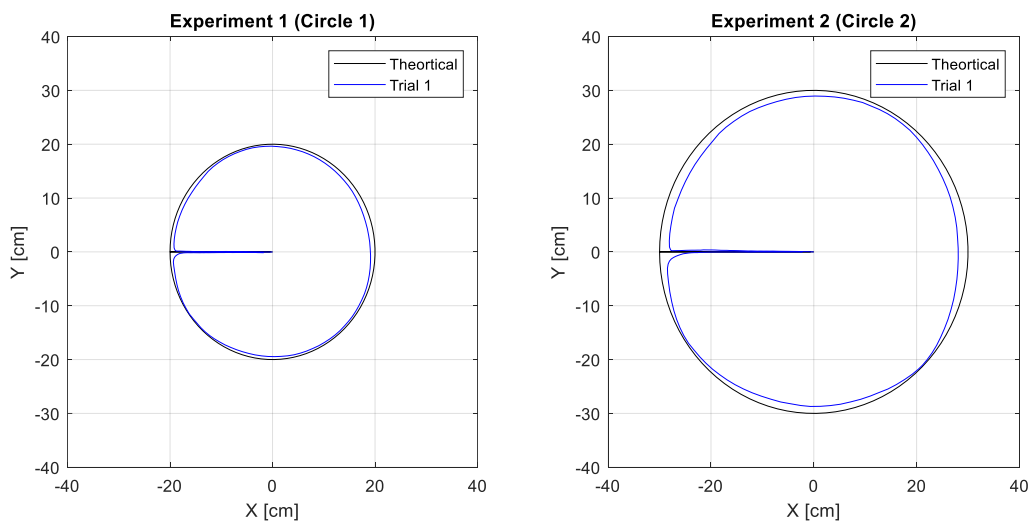


Figure 50: Case 9: study of two circles

The error of motor positioning is larger in the case of the large circle as shown in Figure 51 & 52, which can be attributed to the fact that the number of seeds is constants even though the length of travel has been increased. There is no key observation remark in the speed of both experiments in Figure 53. Experiment two has reached to the higher level, which is reasonable due to the larger path that experiment 2 has.

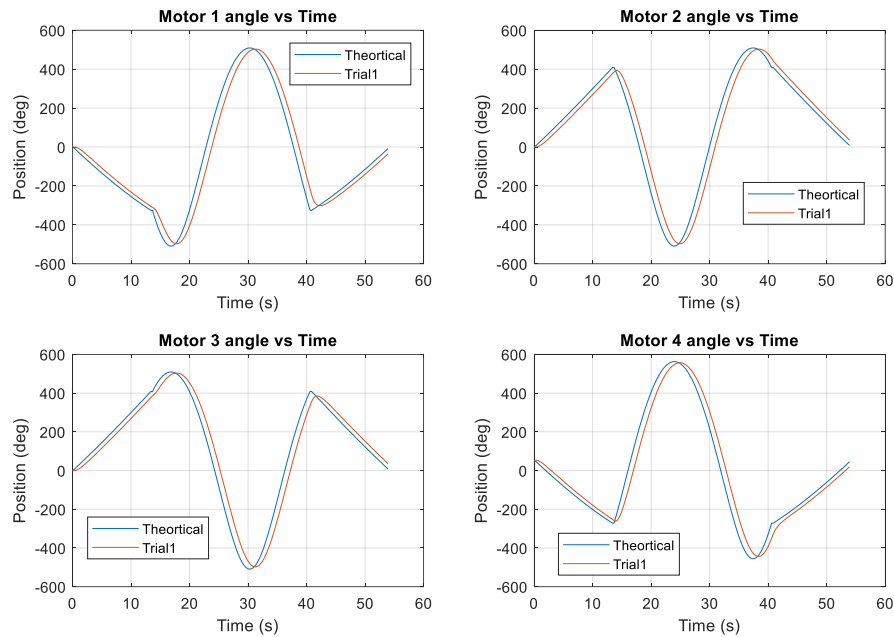


Figure 51: Experiment 1 motor positioning case 9

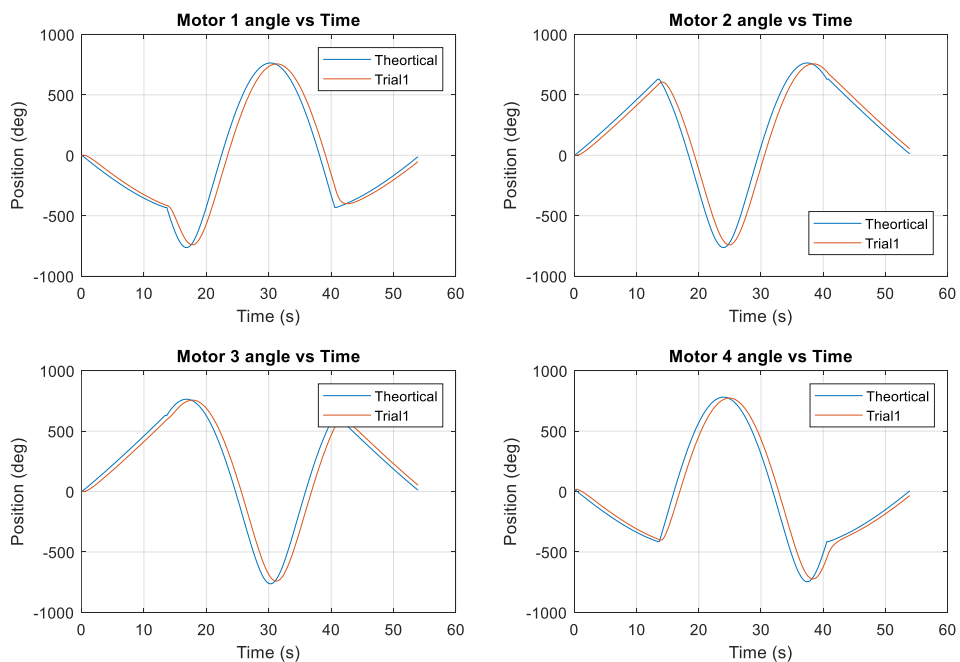


Figure 52: Experiment 2 motor positioning case 9

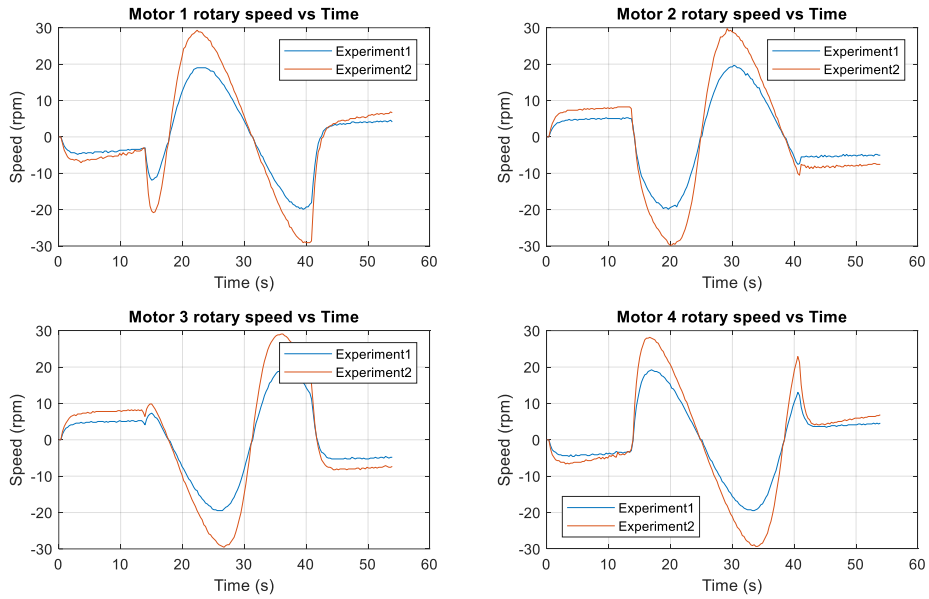


Figure 53: Rotary speed of experiment 1 & 2 case 9

The current measurements of the motors (Figure 54) for both experiments have a lot of ripples, and experiment 2 has more noise compared to experiment 1

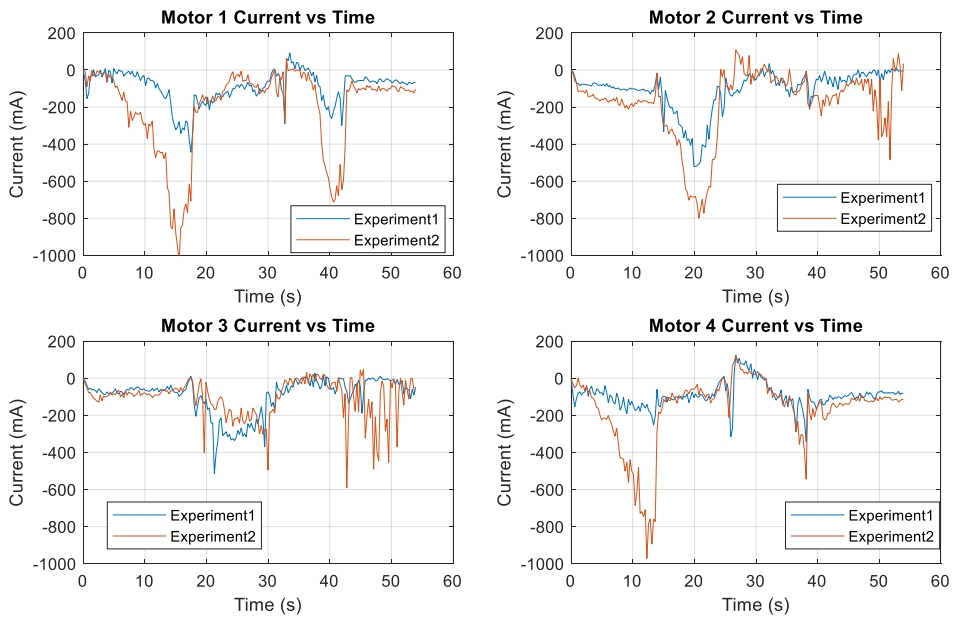


Figure 54: Current profiles of case 9

Due to the lag in the motor command, the experiments have a larger error in the areas where there is a sudden changes (Figure 55-58).

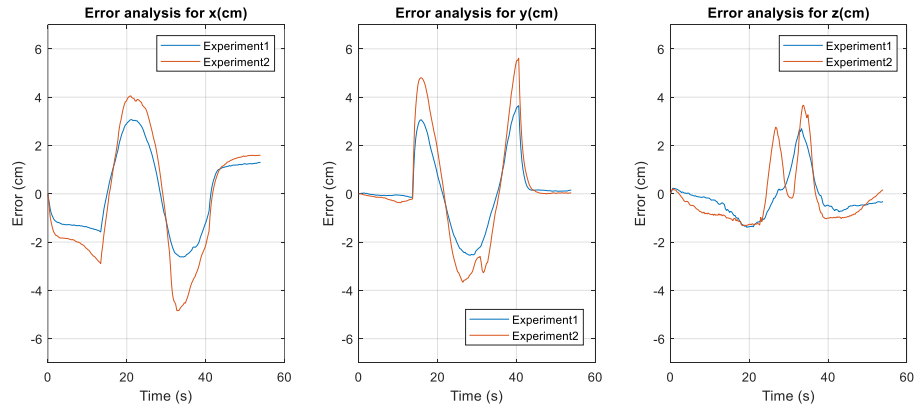


Figure 55: Error signal of case 9

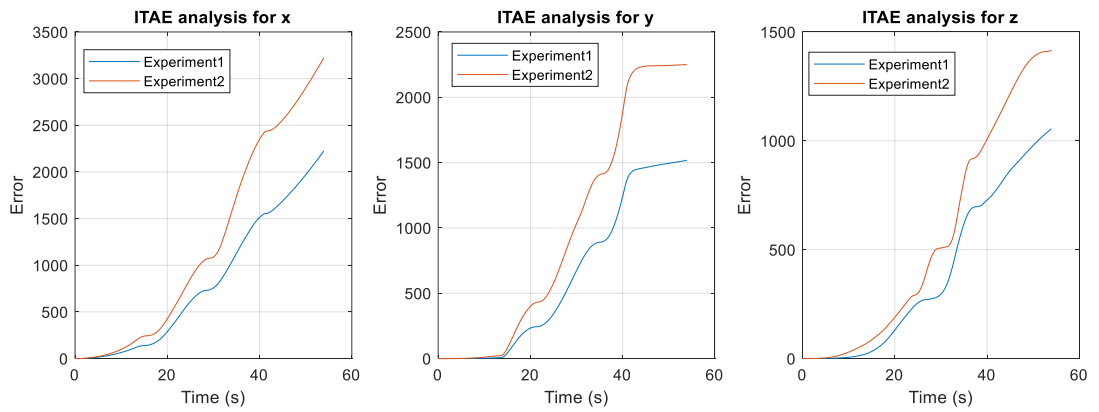


Figure 56: ITAE analysis for case 9

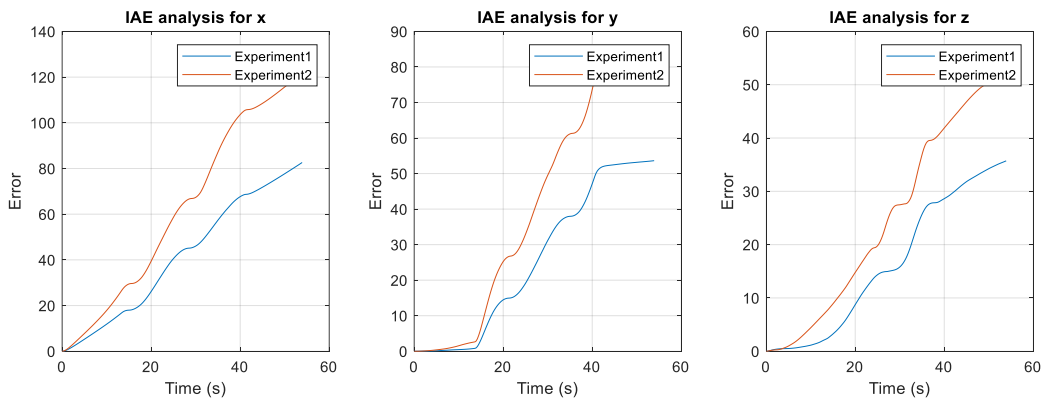


Figure 57: IAE analysis for case 9

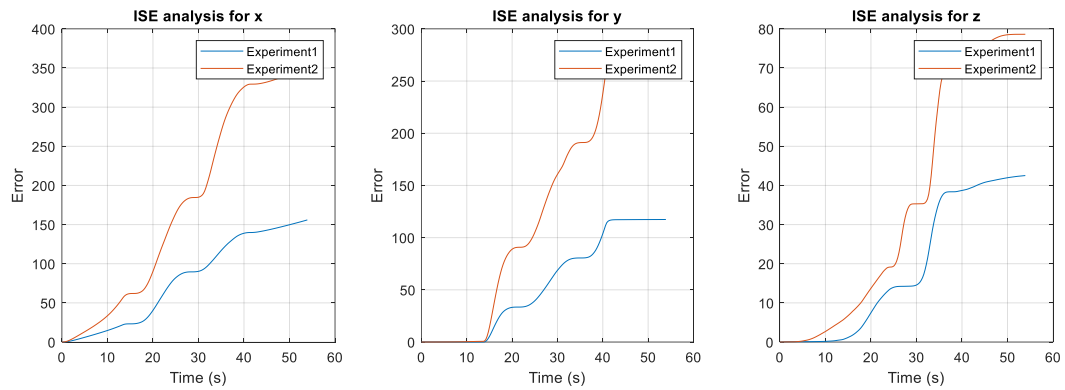


Figure 58: ISE analysis for case 9

The system has more error when the path is larger, which might suggest that the model might not be correct for the extreme points

4.2.10. Case 10

In this case (Figure 59), trapezoidal profile of velocity has been selected a trapezoidal velocity profile has been selected (229-rpm velocity, 37.45rad/s^2 acceleration), and 50 seed number has been selected for the system. Same as case 9, largest circle endures largest error. The position of the largest oval has the largest deviation, which can be attributed to the trapezoidal profile of trajectory between the via points and relatively low number of seeds for path definition. The experiment 1 has the lowest ripple while the experiment 3 has the highest ripples, indicating the fact that the via points in experiment 3 are close to each other. The experiment 1 does not have sudden change in their motion and hence, the change in current is not significant. However, experiment 2 and experiment 3 exhibits some rapid changes, which ultimately lead to impact to the system. The error in signals indicate that the system endures a systematic problem, possibly from lagging of the motor, or due to calibration issues. In the error performance analysis, in x and z directions experiment 2 has the highest error performance number value, whereas in the y direction experiment 3 has the highest value.

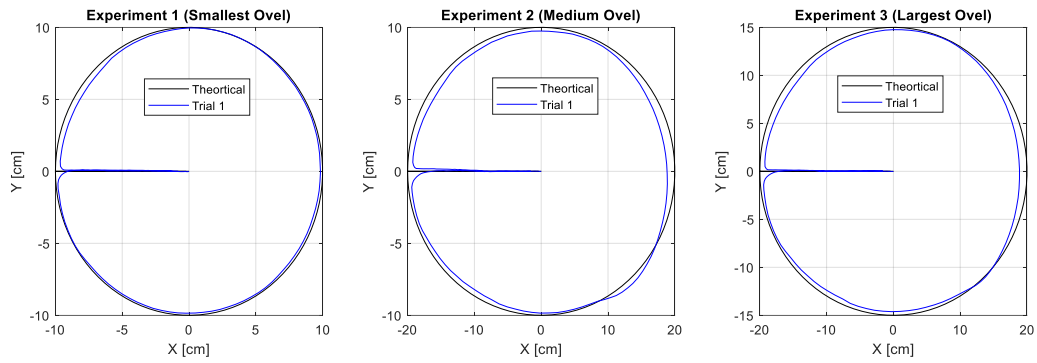


Figure 59: Path generated in case 10

4.2.11. Case 11

In the case 11 (Figure 60), a rectangular shape has been selected, so that the effect of movement in a straight line as well as effect on sharp corners studied. To move between the via points a trapezoidal profile has been selected with parameters of 229-rpm velocity, 37.45rad/s^2 acceleration has been set. The path is made of 100 points or seeds in all three cases. The robot follows the path with a small lag in all three cases (as shown in Figure 61-63) and no significant behavior has been observed. Nonetheless, current ripples in signal have been observed in all three cases (Figure 64). Experiment 3 which is the largest rectangular movement has the highest speed among all three cases.

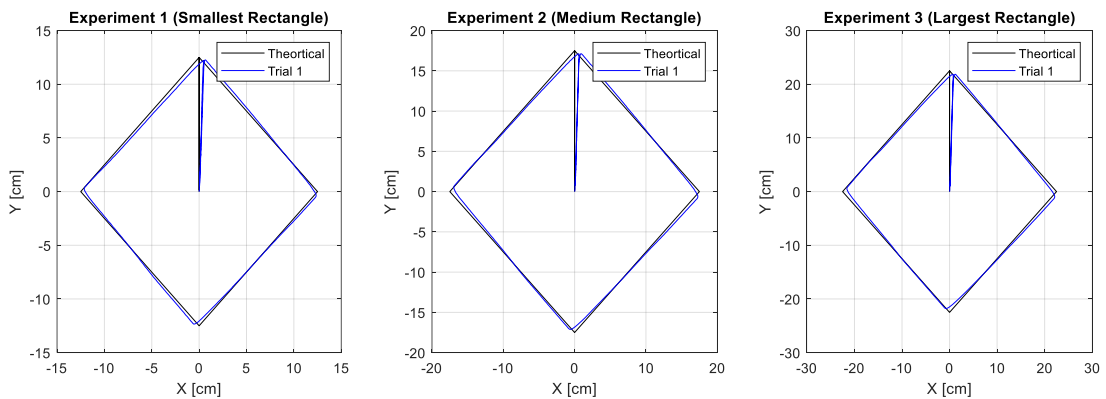


Figure 60: Rectangular Path case 11

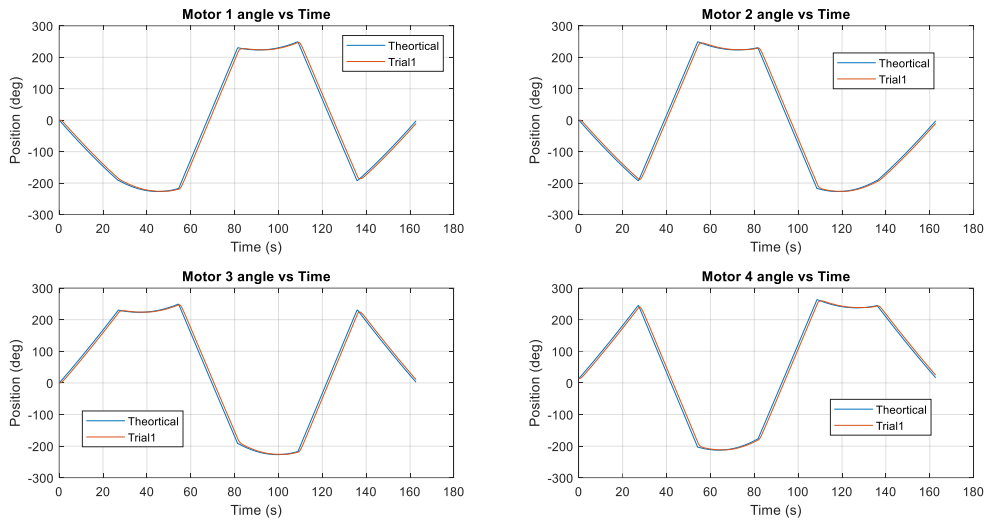


Figure 61: Experiment 1 case 11

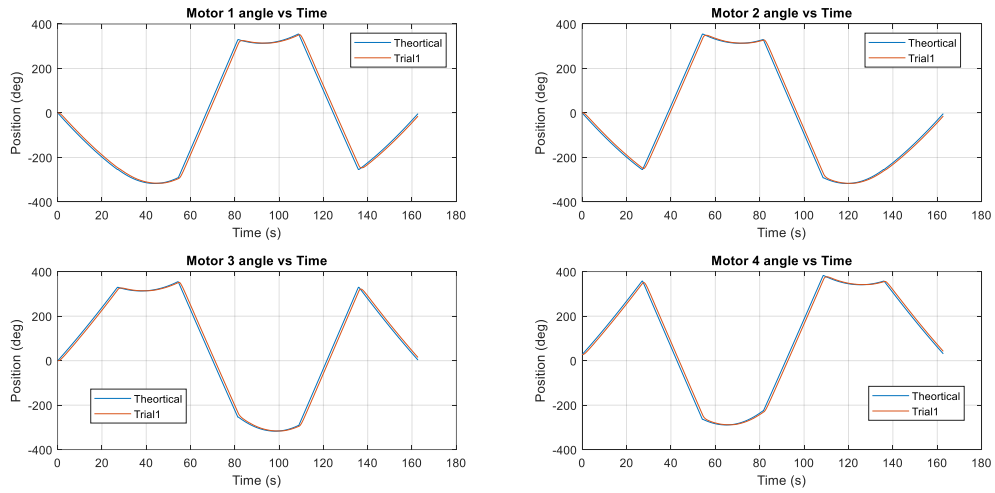


Figure 62: Experiment 2 case 11

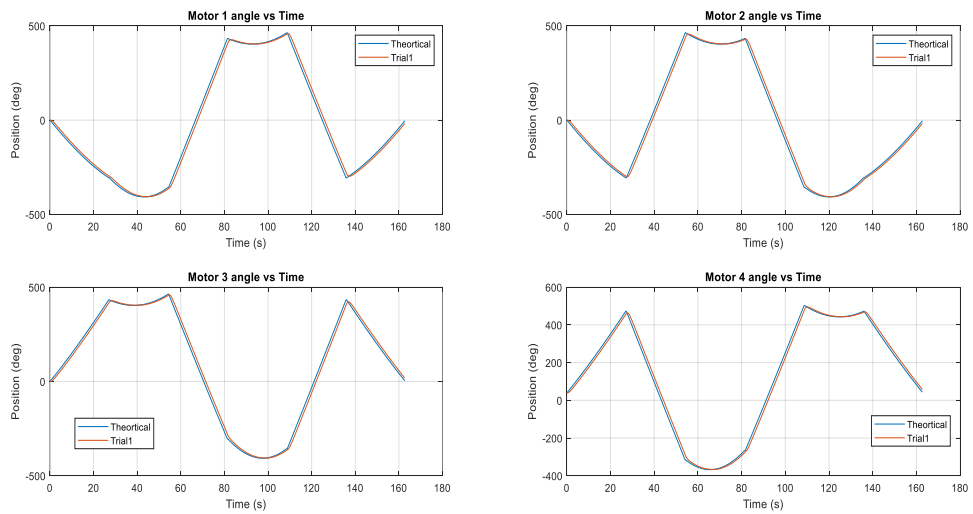


Figure 63: Experiment 3 case 11

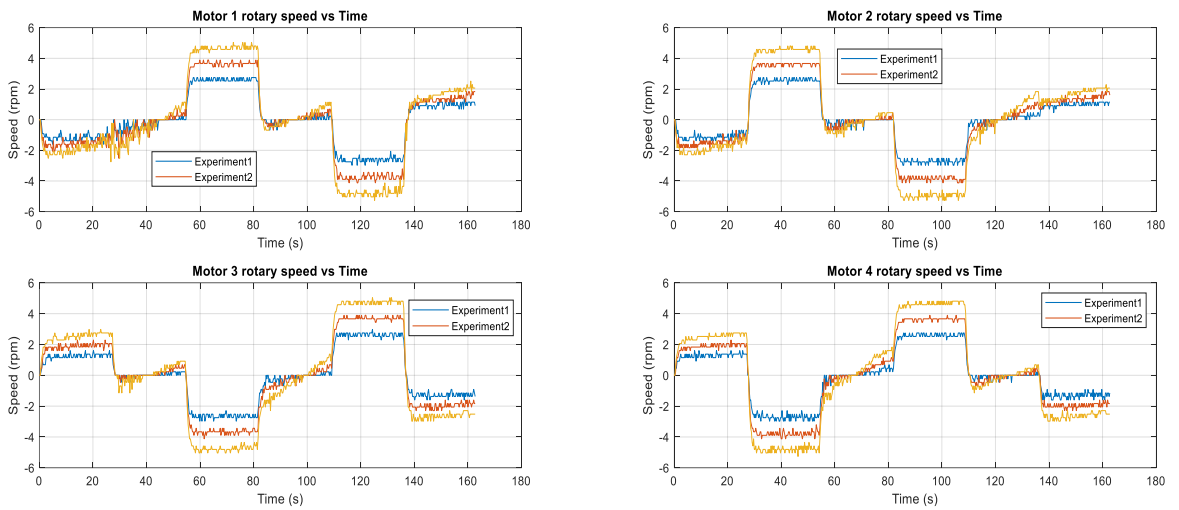


Figure 64: Rotary speed of motor case 11

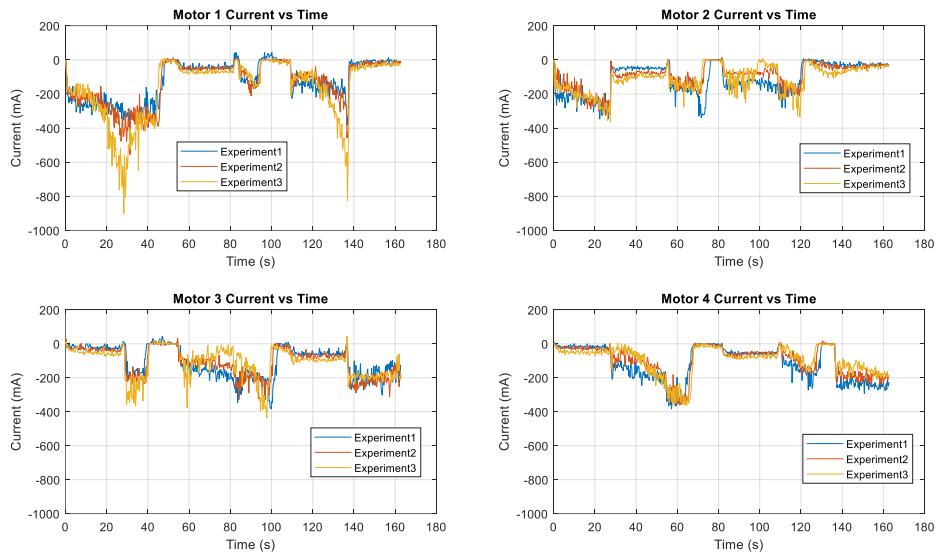


Figure 65: Current profile in case 11

The current signals in case 11 have a lot of noise and does not show any specific pattern., there is a sudden spike of current in places where there is a sharp change in movement. It has been understood that the experiment 3 has the highest error signal (Figure 66-69), which can be due to lag in following the path as well as highest inaccuracy in modeling.

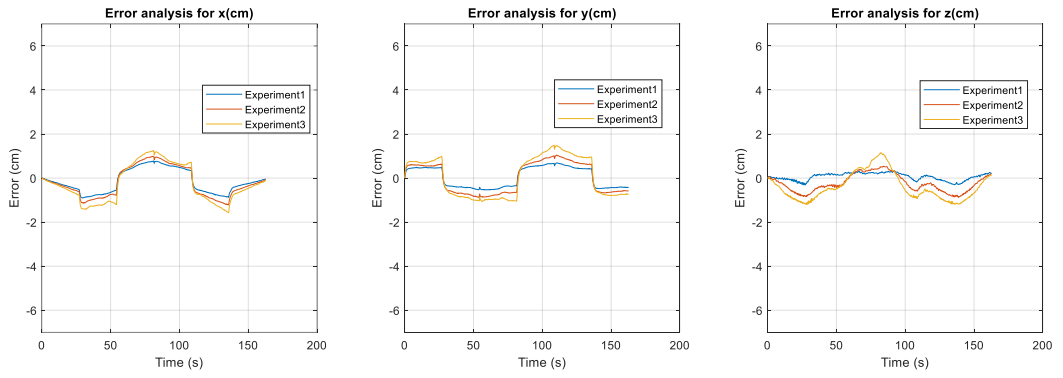


Figure 66: Error signal in case 11

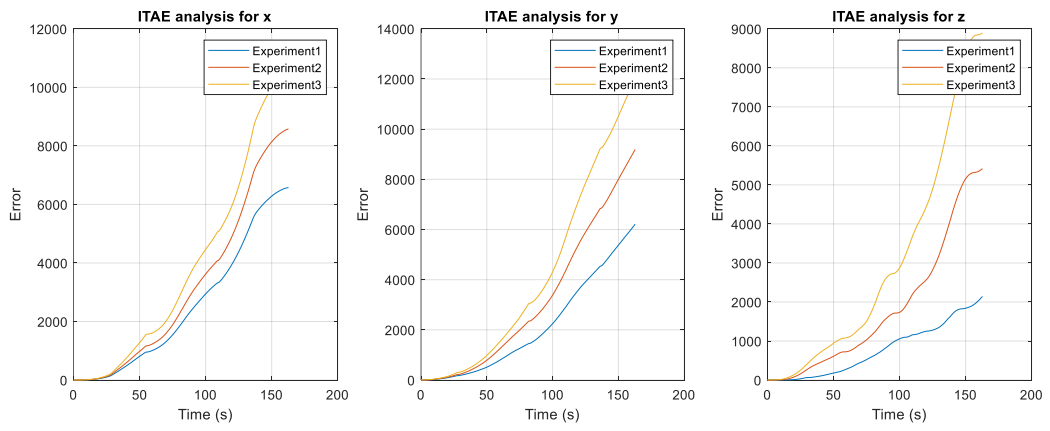


Figure 67: ITAE analysis for case 11

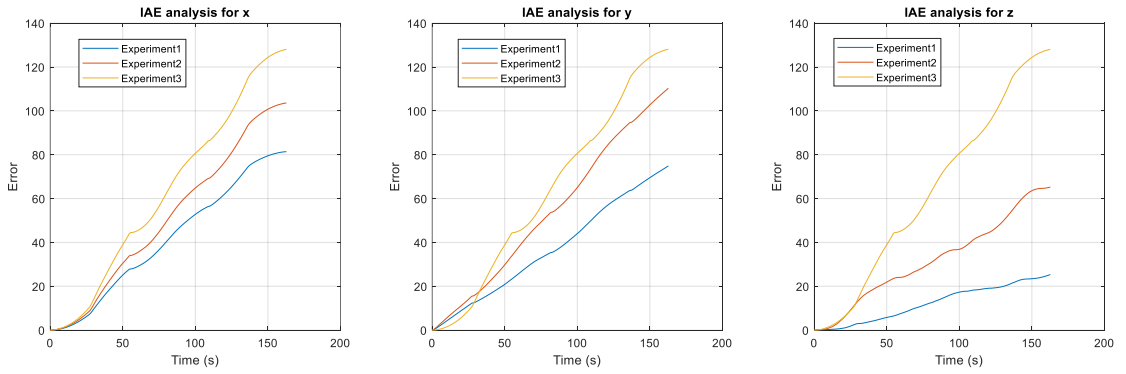


Figure 68: IAE analysis for case 11

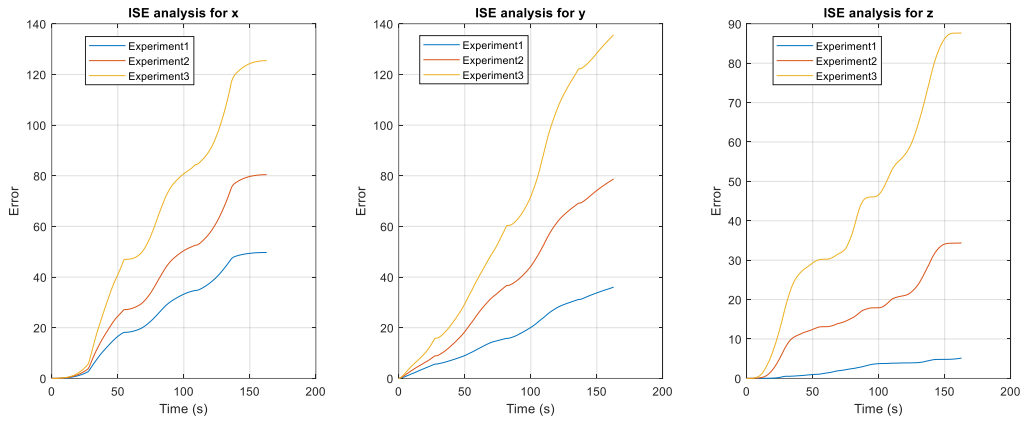


Figure 69: ISE analysis for case 11

In all three-error performance analysis, it has been understood that the larger the size of the rectangle, the higher the error is. Which also supports that model needed to be recalibrated for the cases that are closer to the reach points.

4.2.12. Discussion

Joint control method can follow the given trajectory based on simple or complex mathematical model which describes the system parameters. Complex model will introduce more calculation time and add more requirements for system measurements. In a meantime, simpler models are less-calculation expensive and less dependent on additional sensors. Nonetheless, the limits and accuracy of this method should be calculated through different scenarios to know what the major sources are of in accuracies. This has been done through measurements of the ISE, IAE and ITAE parameters. While ISE penalized errors that are due to steady state response, ITAE penalize the errors due to the transient behavior, such as ripples and oscillations. IAE penalize both transient and steady state response neutrally.

Through studying of 11 cases, it has been demonstrated that the low value of acceleration/deceleration will lead to better steady state response as it is shown in the ISE values of case 3 in Table 7. The model created for this system, however, does not take account of the change in pulley size, which yields to more error in steady state response when the pulley size value is not adjusted in the model, such as case 9. The system exhibits a better transient response when distance between the via points are larger. Uncalibrated system and jerky motions seem to have the most influence errors due to the transient response.

Table 7: Error performance measures comparison

Case #	ISEx	ISEy	ISEz	IAEx	IAEy	IAEz	ITAE _x (10 ³)	ITAE _y (10 ³)	ITAE _z (10 ³)
1	109.1	49.2	433	91.7	65.9	180.	5.5	3.5	8.9
2	79.9	118.5	110.1	84.3	94.4	94.0	3.8	4.6	5.7
3	4.42	12.9	25.3	18.2	27.4	46.3	1.1	1.2	1.1
4	7.6	14.6	56	24.6	28.8	63.1	1.3	1.1	4.0
5	52.2	54.4	67.0	75.6	65.1	72.3	3.8	3.2	3.5
6	57.5	29.5	33.7	72.3	46.3	46.3	1.1	1.1	1.1
7	124.6	154.0	84.5	74.7	78.2	58.7	1.8	2.1	1.6
8	180.0	204.5	186.2	61.0	65.2	59.7	0.7	0.9	0.7
9	352.2	270.5	78.6	121.8	82.4	50.9	3.2	2.2	1.4
10	86.4	39.1	72.0	86.4	39.1	56.6	2.3	1.1	2.0
11	128.1	143.2	106.5	125.5	135.6	87.7	1.1	1.1	1.1

The values of the Mean Square Error (MSE) for this experiment indicates that the error is largest in the x axis, which indicates that the inverse kinematic model along x axis needed to be adjusted and modified. As shown in Table 8, the value of MSE for y axis is higher in case 2, 7, 8, 9, which can be attributed to the fact that the error might be due to calibration or incorrect modeling. The values of the MSE in z axis are lowest since the trajectory does not consider any movement in this direction. The error in z axis can be attributed to the fact that there is not enough pretension in the cables or modeling parameters are incorrect in this direction.

Table 8: Mean square error for the different experiments

Case #	MSE _x	MSE _y	MSE _z
1	0.0198546	4.54166×10 ⁻⁵	0.000399354
2	0.0788248	0.000109321	0.00010141
3	0.0796382	1.18746×10 ⁻⁵	2.33231×10 ⁻⁵
4	0.0794159	1.34455×10 ⁻⁵	5.16083×10 ⁻⁵
5	0.0790509	5.01423×10 ⁻⁵	6.17174×10 ⁻⁵
6	0.0792292	2.72039×10 ⁻⁵	3.10304×10 ⁻⁵
7	0.0784167	0.000285122	0.000156169
8	0.0776027	0.000763138	0.000692195
9	0.145861	0.000499803	0.000145248
10	0.0655273	6.25239×10 ⁻⁵	0.000244869
11	0.04491	8.33048×10 ⁻⁵	5.3809×10 ⁻⁵

Experiments carried out in this study has shown that the control joint method in conjecture with geometric inverse kinematic model can be an affective scheme to for control of the cable robot. Certain drawbacks in the system can be attributed to the fact that the system needed to be calibrated periodically due to inaccuracy in the system model parameters and lack of control scheme at the higher level. The higher level control can be achieved by Opti-track cameras real-time measurements and proper control scheme based on the values received by the cameras.

Chapter 5. Conclusion

The cable driven parallel cable robots (CDPR) characteristics, such as high payload-to-weight ratio and flexibility, have led researchers to explore its potential in several applications, such as biomedical devices. While flexible links in CDPR can reduce the cost and energy consumption, the modeling and control of the system can be a cumbersome task due to the nonlinearity of the system and unilateral conditions. In this study, A CDPR with 1R2T configuration has been studied for head-neck rehabilitation. It has been revealed that the PID control joint method can perform trajectory planning tasks with fair accuracy. Nonetheless, this method is heavily dependent on the accuracy of the model there is no higher level of control for end-effector as a correction factor to the system. The Geometric Inverse Kinematic (GIK) will effectively captures the main features of the robot; hence, the operator can achieve the desire robot movement by implementing this mathematical model to give motor commands. In the studies performed, it has been demonstrated that with slow movement, the ISE value of will reach to a low value as 25.3, and with optimized way of selecting via points, there will be less transient error and ITAE can reached to a low value as 706.2. This method, nonetheless, does not capture changes in the system due to manufacturing errors or uncalibrated system. Further studies can create models that can include uncertainty of the model while designing the controller. In addition, a manikin can be used in further studies to verify the adequacy of this type of robot for human trials.

References

- [1] J.-P. Merlet, *Parallel Robots*, vol. 74. Dordrecht: Springer Netherlands, 2000. doi: 10.1007/978-94-010-9587-7.
- [2] M. Morris and M. Shoham, “Applications and Theoretical Issues of Cable-Driven Robots,” p. 30, 2009.
- [3] H. Xiong and X. Diao, “A review of cable-driven rehabilitation devices,” *Disability and Rehabilitation: Assistive Technology*, vol. 15, no. 8, pp. 885–897, Nov. 2020, doi: 10.1080/17483107.2019.1629110.
- [4] J. E. Muscolino, *Kinesiology: the skeletal system and muscle function*, 2nd ed. St. Louis, Mo: Mosby/Elsevier, 2011.
- [5] L. Lippert and L. Lippert, *Clinical kinesiology and anatomy*, 4th ed. Philadelphia: F.A. Davis, 2006.
- [6] J. Zariffa *et al.*, “Feasibility and efficacy of upper limb robotic rehabilitation in a subacute cervical spinal cord injury population,” *Spinal Cord*, vol. 50, no. 3, pp. 220–226, Mar. 2012, doi: 10.1038/sc.2011.104.
- [7] K. Guru, U. K. Manoor, and S. S. Supe, “A comprehensive review of head and neck cancer rehabilitation: physical therapy perspectives,” *Indian J Palliat Care*, vol. 18, no. 2, pp. 87–97, May 2012, doi: 10.4103/0973-1075.100820.
- [8] H. M. Qassim and W. Z. Wan Hasan, “A Review on Upper Limb Rehabilitation Robots,” *Applied Sciences*, vol. 10, no. 19, p. 6976, Oct. 2020, doi: 10.3390/app10196976.
- [9] D. Shi, W. Zhang, W. Zhang, and X. Ding, “A Review on Lower Limb Rehabilitation Exoskeleton Robots,” *Chin. J. Mech. Eng.*, vol. 32, no. 1, p. 74, Dec. 2019, doi: 10.1186/s10033-019-0389-8.
- [10] H. Zhang, K. Albee, and S. K. Agrawal, “A spring-loaded compliant neck brace with adjustable supports,” *Mechanism and Machine Theory*, vol. 125, pp. 34–44, Jul. 2018, doi: 10.1016/j.mechmachtheory.2017.12.025.

- [11] M. Shoaib, C. Y. Lai, and A. Bab-Hadiashar, “A Novel Design of Cable-Driven Neck Rehabilitation Robot (CarNeck),” in *2019 IEEE/ASME International Conference on Advanced Intelligent Mechatronics (AIM)*, Hong Kong, China, Jul. 2019, pp. 819–825. doi: 10.1109/AIM.2019.8868660.
- [12] P. Lingampally and A. Selvakumar, “A kinematic and workspace analysis of a parallel rehabilitation device for head-neck injured patients,” *FME Transactions*, vol. 47, no. 3, pp. 405–411, 2019, doi: 10.5937/fmet1903405L.
- [13] M. E.-H. Ibrahim, M. S. El- Mohandes, M. T. El-Wakad, and S. A. Sami, “Design and Analysis of a Dynamic Neck Brace,” in *2021 3rd Novel Intelligent and Leading Emerging Sciences Conference (NILES)*, Giza, Egypt, Oct. 2021, pp. 236–240. doi: 10.1109/NILES53778.2021.9600507.
- [14] J. Liu, Y. Cheng, S. Zhang, Z. Lu, and G. Gao, “Design and Analysis of a Rigid-Flexible Parallel Mechanism for a Neck Brace,” *Mathematical Problems in Engineering*, vol. 2019, pp. 1–20, Nov. 2019, doi: 10.1155/2019/9014653.
- [15] B.-C. Chang, H. Zhang, S. Long, A. Obayemi, S. H. Troob, and S. K. Agrawal, “A novel neck brace to characterize neck mobility impairments following neck dissection in head and neck cancer patients,” *Wearable Technol.*, vol. 2, p. e8, 2021, doi: 10.1017/wtc.2021.8.
- [16] W. Yang Ho, W. Kraus, A. Mangold, and A. Pott, “Haptic Interaction with a Cable-Driven Parallel Robot Using Admittance Control,” in *Cable-Driven Parallel Robots*, Cham, 2015, pp. 201–212.
- [17] J.-B. Izard, M. Gouttefarde, C. Baradat, D. Culla, and D. Sallé, “Integration of a Parallel Cable-Driven Robot on an Existing Building Façade,” in *Cable-Driven Parallel Robots*, vol. 12, T. Bruckmann and A. Pott, Eds. Berlin, Heidelberg: Springer Berlin Heidelberg, 2013, pp. 149–164. doi: 10.1007/978-3-642-31988-4_10.
- [18] P. Zhuang and Z. Yao, “Dynamics and control of cable-suspended parallel robots for giant telescopes,” presented at the SPIE Astronomical Telescopes + Instrumentation, Orlando, Florida , USA, Jun. 2006, p. 62673H. doi: 10.1117/12.669937.
- [19] T. P. Tho and N. T. Thinh, “Using a Cable-Driven Parallel Robot with Applications in 3D Concrete Printing,” *Applied Sciences*, vol. 11, no. 2, p. 563, Jan. 2021, doi: 10.3390/app11020563.

- [20] A. Alamdari, R. Haghghi, and V. Krovi, “Stiffness Modulation in an Elastic Articulated-Cable Leg-Orthosis Emulator: Theory and Experiment,” *IEEE Trans. Robot.*, vol. 34, no. 5, pp. 1266–1279, Oct. 2018, doi: 10.1109/TRO.2018.2830356.
- [21] W. M. Nunes, L. A. O. Rodrigues, L. P. Oliveira, J. F. Ribeiro, J. C. M. Carvalho, and R. S. Goncalves, “Cable-based parallel manipulator for rehabilitation of shoulder and elbow movements,” in *2011 IEEE International Conference on Rehabilitation Robotics*, Zurich, Jun. 2011, pp. 1–6. doi: 10.1109/ICORR.2011.5975503.
- [22] F. Ennaiem *et al.*, “A Reconfigurable 6-DoF Cable-Driven Parallel Robot with an Extended Rotational Workspace,” in *Mechanism Design for Robotics*, vol. 103, S. Zegloul, M. A. Laribi, and M. Arsicault, Eds. Cham: Springer International Publishing, 2021, pp. 322–331. doi: 10.1007/978-3-030-75271-2_34.
- [23] T. Bruckmann, L. Mikelsons, T. Brandt, M. Hiller, and D. Schramm, “Wire Robots Part I: Kinematics, Analysis & Design,” in *Parallel Manipulators, New Developments*, J.-H. Ryu, Ed. I-Tech Education and Publishing, 2008. doi: 10.5772/5365.
- [24] A. A. Kumar, J.-F. Antoine, P. Zattarin, and G. Abba, “Workspace Analysis of a 4 Cable-Driven Spatial Parallel Robot,” in *ROMANSY 22 – Robot Design, Dynamics and Control*, vol. 584, V. Arakelian and P. Wenger, Eds. Cham: Springer International Publishing, 2019, pp. 204–212. doi: 10.1007/978-3-319-78963-7_27.
- [25] L. Gagliardini, M. Gouttefarde, and S. Caro, “Determination of a Dynamic Feasible Workspace for Cable-Driven Parallel Robots,” in *Advances in Robot Kinematics 2016*, vol. 4, J. Lenarčič and J.-P. Merlet, Eds. Cham: Springer International Publishing, 2018, pp. 361–370. doi: 10.1007/978-3-319-56802-7_38.
- [26] T. Paty, N. Binaud, S. Caro, and S. Segonds, “Cable-driven parallel robot modelling considering pulley kinematics and cable elasticity,” *Mechanism and Machine Theory*, vol. 159, p. 104263, May 2021, doi: 10.1016/j.mechmachtheory.2021.104263.
- [27] A. B. Alp and S. K. Agrawal, “Cable suspended robots: design, planning and control,” in *Proceedings 2002 IEEE International Conference on Robotics and Automation (Cat. No.02CH37292)*, Washington, DC, USA, 2002, vol. 4, pp. 4275–4280. doi: 10.1109/ROBOT.2002.1014428.

- [28] R. Mersi, S. Vali, M. S. haghghi, G. Abbasnejad, and M. T. Masouleh, "Design and Control of a Suspended Cable-Driven Parallel Robot with Four Cables," in *2018 6th RSI International Conference on Robotics and Mechatronics (ICRoM)*, Tehran, Iran, Oct. 2018, pp. 470–475. doi: 10.1109/ICRoM.2018.8657534.
- [29] S. A. Khalilpour, H. D. Taghirad, and H. Habibi, "Wave-based control of suspended cable driven parallel manipulators," in *2017 5th International Conference on Control, Instrumentation, and Automation (ICCIA)*, Shiraz, Nov. 2017, pp. 173–178. doi: 10.1109/ICCIAutom.2017.8258673.
- [30] M. I. Hosseini, M. J. Harandi, S. A. Khalilpour Seyedi, and H. reza Dokht taghirad, "Adaptive Fast Terminal Sliding Mode Control of A Suspended Cable-Driven Robot," in *2019 27th Iranian Conference on Electrical Engineering (ICEE)*, Yazd, Iran, Apr. 2019, pp. 985–990. doi: 10.1109/IranianCEE.2019.8786501.
- [31] B. Jung and B. S. Bhutta, *Anatomy, Head and Neck, Neck Movements*. StatPearls Publishing, Treasure Island (FL), 2022. [Online]. Available: <http://europepmc.org/abstract/MED/32491487>
- [32] S. Rahman and J. M Das, *Anatomy, Head and Neck, Cervical Spine*. StatPearls Publishing, Treasure Island (FL), 2022. [Online]. Available: <http://europepmc.org/abstract/MED/32491448>
- [33] W. Graf, C. D. Waele, and P. P. Vidal, "Functional anatomy of the head-neck movement system of quadrupedal and bipedal mammals," *Great Britain*, pp. 55–74, 1995.
- [34] V. F. Ferrario, C. Sforza, G. Serrao, G. Grassi, and E. Mossi, "Active range of motion of the head and cervical spine: a three-dimensional investigation in healthy young adults," *J. Orthop. Res.*, vol. 20, no. 1, pp. 122–129, Jan. 2002, doi: 10.1016/S0736-0266(01)00079-1.
- [35] A. J. Moreno, G. Utrilla, J. Marin, J. J. Marin, M. B. Sanchez-Valverde, and A. C. Royo, "Cervical Spine Assessment Using Passive and Active Mobilization Recorded Through an Optical Motion Capture," *Journal of Chiropractic Medicine*, vol. 17, no. 3, pp. 167–181, Sep. 2018, doi: 10.1016/j.jcm.2017.12.004.
- [36] D. R. Peterson and J. D. Bronzino, Eds., *Biomechanics: principles and applications*. Boca Raton: CRC Press, 2008.

- [37] Z. Zhang *et al.*, “State-of-the-art on theories and applications of cable-driven parallel robots,” *Front. Mech. Eng.*, vol. 17, no. 3, p. 37, Sep. 2022, doi: 10.1007/s11465-022-0693-3.
- [38] X. Jin, J. Jung, S. Ko, E. Choi, J.-O. Park, and C.-S. Kim, “Geometric Parameter Calibration for a Cable-Driven Parallel Robot Based on a Single One-Dimensional Laser Distance Sensor Measurement and Experimental Modeling,” *Sensors*, vol. 18, no. 7, p. 2392, Jul. 2018, doi: 10.3390/s18072392.
- [39] ROBOTIS, “ROBOTIS e-Manual: mx-64.” ROBOTIS, 2022. [Online]. Available: <https://emanual.robotis.com/docs/en/dxl/mx/mx-64/>

Vita

Mohammad Latifi was born in 1995, in Tehran, Iran. He received his primary and secondary education in Dubai, UAE. He received his B.Sc. degree in Electrical and Electronic Engineering from the American University of Sharjah in 2019.

In September 2020, he joined the Mechatronic Engineering master's program in the American University of Sharjah as a graduate teaching assistant. During his master study, he developed a method intelligent system for crop health detection, for which his project was selected as a runner-up in James Dyson competition. His research interests are mathematical modelling, kinematic and machine design, computer vision, and biomedical robots.